IEEE Access
Multidisciplinary | Rapid Review | Open Access Journal

Received November 5, 2021, accepted November 22, 2021, date of publication November 29, 2021,
date of current version December 9, 2021.

*Digital Object Identifier 10.1109/ACCESS.2021.3131161*

# A Bio-Inspired Heuristic Algorithm for Solving Optimal Power Flow Problem in Hybrid Power System

**MANZOOR AHMAD[1], NADEEM JAVAID[1,2], (Senior Member, IEEE), IFTIKHAR AZIM NIAZ[1], (Senior Member, IEEE), AHMAD ALMOGREN[3], (Senior Member, IEEE), AND AYMAN RADWAN[4], (Senior Member, IEEE)**

[1]Department of Computer Science, COMSATS University Islamabad, Islamabad 44000, Pakistan
[2]School of Computer Science, University of Technology Sydney, Ultimo, NSW 2007, Australia
[3]Department of Computer Science, College of Computer and Information Sciences, King Saud University, Riyadh 11633, Saudi Arabia
[4]Instituto de Telecomunicacoes, Universidade de Aveiro, 3810-193 Aveiro, Portugal

Corresponding authors: Nadeem Javaid (nadeemjavaidqau@gmail.com) and Ahmad Almogren (ahalmogren@ksu.edu.sa)

This work was supported by King Saud University, Riyadh, Saudi Arabia, through Researchers Supporting under Project RSP-2021/184. The work of Ayman Radwan was supported in part by the FCT / MEC through Programa Operacional Regional do Centro, and in part by the European Union through the European Social Fund (ESF) under Investigador FCT under Grant 5G-AHEAD IF/FCT-IF/01393/2015/CP1310/CT0002.

**ABSTRACT** In recent studies, emphasis has been placed on optimal power flow (OPF) problems in traditional thermal, wind, and solar energy sources-based hybrid power systems. Various metaheuristic algorithms have been proposed to find optimal solutions to the OPF problems in the hybrid power system. The OPF, due to the quadratic nature of its primary objective function, is a nonlinear, nonconvex, and quadratic optimization problem. In this study, we have proposed a bio-inspired bird swarm algorithm (BSA) to find an optimal solution to the OPF problem in the hybrid power system because it performs well in the case of optimizing the well-known Rastrigin quadratic benchmark function. In this study, uncertainty of utility load demand and stochastic electricity output from renewable energy resources (RESs) including wind and solar are incorporated into the hybrid power system for achieving accuracy in operations and planning of the system. We have used a modified IEEE-30 bus test system to verify and measure the performance of BSA and a comparison is made with well-known evolutionary metaheuristic algorithms. The proposed BSA consistently achieves more accurate and stable results than other metaheuristic algorithms. Simulation-based optimization results have shown the superiority of BSA approach to solve the OPF problems by satisfying all constraints and minimum power generation cost 863.121 $/h is achieved in case study 1. Simulation-based experiment results have indicated that by imposing the carbon tax ($ton/h$) the power generation from RESs was increased. In case study 2, the proposed BSA approach has also outperformed and minimum electricity cost 890.728 $/h is achieved as compared to other algorithms.

**INDEX TERMS** Deterministic optimal power flow, uncertainty of utility load demand, bio-inspired bird swarm algorithm, stochastic solar and wind power.

## I. INTRODUCTION

### A. BACKGROUND AND MOTIVATION

Generally, an electric power grid or power system consists of power generation plants, electricity transmission and distribution systems. The power generation plants generate electrical power through electricity generation units or power plants. The transmission system carries the electricity through transmission lines from electricity generation plants to utilities or load centers. The electricity distribution system feeds the electricity through distribution lines to nearby homes, agricultural units, industries, and commercial buildings. The traditional electric power grids are responsible for producing electricity and carrying it to residential, industrial, and

The associate editor coordinating the review of this manuscript and approving it for publication was Ahmed F. Zobaa.

commercial consumers through electricity transmission and distribution lines. Two authorities, 1) independent system operator (ISO) and 2) electric utility, are responsible to control operations and planning of the power system in a country. The ISO is an independent authority established by the government to ensure reliability of electricity generation and the transmission system in the electrical power grid. An electric utility is an authority that engages in feeding the electricity through distribution lines to consumers by balancing the demand and supply of the electrical load.

In the electrical power grid operations and planning, the control always resides on the generation side and the power generation plants adjust their electricity generation according to the changes in electricity demand from consumers. Sometimes power generation plants produce surplus electricity, which is transmitted to the nearby area by transmission lines or stored [1]. Therefore, it is of practical importance to balance load demand and electricity supply in the power system. For this purpose, many techniques have been applied in the research literature. On the generation side, to address optimal power flow (OPF) problems in the power system is considered as a technique for finding stable and secure operating points of electricity generation plants and their optimal scheduling on an hourly basis [2]–[5].

In 1962, Carpentier first introduced economic dispatch problem extension as the OPF problem in traditional thermal energy sources-based power systems [6]. The OPF is one of the well-known and well-studied research areas in the power system. It can be defined as: *"To find out the stable and secure operating points (levels) for electricity generation plants in order to meet load demand of utility in power system, generally with attention to minimize electricity generation cost"* [6]. In traditional thermal energy sources-based power systems, the OPF is a nonconvex, nonlinear, and quadratic problem due to the quadratic nature of its primary objective function to reduce electricity generation cost. The primary objective function of OPF problem has been modeled as quadratic curve and its various forms such as valve-point loading effect quadratic curve, piecewise quadratic curve, and prohibited operating zones quadratic curve for the traditional thermal energy source [6], [7]. Researchers have also proposed various techniques for solving the OPF problems considering other objectives, in addition to the primary electricity generation cost minimization objective. These objectives include minimizing voltage deviation, power loss in transmission lines, and emission pollution and enhancing voltage stability index [6]–[9].

In the last decade, integration of environment friendly and clean electricity output from renewable energy sources (RESs) including wind and solar into thermal power systems have become necessary due to the rising demand for electricity and global warming issues. Therefore, the power systems are striving towards a sustainable system future due to rapidly growing integration of RESs in power systems. On the electricity generation side, the RESs such as solar photovoltaic (PV) units and windfarms are being owned by private parties in a power system. The ISO purchases scheduled renewable electricity from private parties in order to cater the growing consumers' load demand. Wind power generation depends upon stochastic wind speed at different times of day. Similarly solar PV power generation depends upon uncertain solar irradiance during the day time. Due to the fluctuant and intermittent solar and wind power output, the available power from solar PV units and windfarms may be more or less than wind-scheduled power at different times of day. In an overestimation scenario, the ISO is required to have a spinning reserve based on utility load demand, when power supplied by solar PV units and windfarms operators is less than wind-scheduled power. The ISO has to increase the reserve cost associated with reserve electricity generation units to balance the supply and demand in this scenario. An underestimation scenario may arise when actual renewable energy received from RESs is greater than scheduled power. In that case, the surplus power output from RESs is wasted and ISO bears a penalty cost if it is not stored or transmitted to a nearby area [8], [9]. Incorporating stochastic power generation from wind and solar into the system raises the complexity of power system operations and planning. The utility load demand is also uncertain in nature due to variation in consumers' load demand that directly affects spinning reserve cost in the power system. Moreover, considering the uncertainty of utility load demand has significant importance to achieve accuracy in the operations and planning of the system. Therefore, an effective technique is required to reduce the overall electricity generation cost.

### B. LITERATURE REVIEW

In the research literature, various studies have been documented using two types of optimization algorithms for solving the OPF problems in the power system. These optimization algorithm types are traditional mathematical algorithms or methods and metaheuristic algorithms. Numerous mathematical optimization methods including linear programming [10], linear/quadratic programming [11], sequential linear programming [12], newton method [13], generalized benders decomposition (GBD) [14], nonlinear programming [15]–[17], mixed integer nonlinear programming (MINLP), [18], interior point method [19], [20], and simplified gradient method [21] have been applied to solve the OPF problems. In these traditional methods, nonlinear objective function and constraints are converted into linear form before solving the OPF problem because the mathematical method cannot handle the nonlinear properties of the problem [22]. This convergence in constraints and objective functions may affect the accuracy of operations and planning of the power system.

The OPF problem in thermal energy sources-based power systems widely has been studied by researchers using metaheuristic algorithms. In the last decade, numerous studies have been documented based on metaheuristic algorithms such as binary backtracking search algorithm (BBSA) [6], adaptive group search optimization (AGSO) [23], improved

colliding bodies optimization (ICBO) [25], differential search algorithm (DSA) [24], moth swarm algorithm (MSA) [26], stud krill herd (SKH) [27], [28], differential evolution (DE) [29], hybrid of genetic algorithm (GA) and PSO [30], GA based on multi-parent crossover (GA-MPC) [31], improved social spider optimization (ISSO) [32], modified grasshopper optimization (MGO) [33], improved moth flame optimization (IMFO) [34], multi-objective EA based decomposition (MOEA/D) [35], modified pigeon-inspired optimization (MPIO) [36], and adaptive moth flame optimization (AMFO) [37] to find optimal solutions to the OPF problems in traditional power systems. The abbreviation of different terms and methods are specified in Table 1.

The OPF problem primary objective – electricity generation cost minimization, is considered in all of the aforementioned studies [6], [23]–[37]. Moreover, other objectives such as reducing power loss in transmission lines, emission pollution, etc. are considered in some studies. In these studies, the performance of proposed metaheuristic algorithms has been measured on one or more IEEE-30, IEEE-57 and IEEE-118, bus test systems. The power systems are rapidly growing with RESs integration due to increasing electricity demand and global warming issue due to traditional thermal energy sources.

In the literature, some studies have been documented [38]–[42] to find optimal solutions to the OPF problems in traditional thermal and wind energy sources-based hybrid power systems with a focus on minimizing the overall cost of electricity generation. In study [38], gbest guided ABC (GABC) has been utilized to find optimal solutions to the OPF problems in the thermal and wind energy sources-based hybrid power systems. In which objectives were to minimize electricity generation cost and emission pollution. In study [39], modified bacteria foraging algorithm (MBFA) is employed for solving the OPF problem in the traditional thermal and wind energy sources-based hybrid power system. A doubly-fed induction generator model is utilized to justify the OPF problem inequality constraints and problem is formulated with various objective functions in above study. In study [40], authors applied ant colony optimization (ACO) and MBFA for solving the OPF problems in the traditional thermal and wind energy sources-based hybrid power systems. In study [41], authors utilized multi-objective glowworm swarm optimization (GWSO) to solve the OPF problems in the thermal and wind energy sources-based hybrid power systems. In all of the aforementioned studies, [38]–[41], the authors have utilized a modified IEEE-30 bus test system to verify and measure performance of the applied approaches. In study [42], the authors have adopted self-adaptive evolutionary programming (EP) for solving the OPF problems in the traditional thermal and wind energy sources-based hybrid power systems. In all of the aforementioned studies [38]–[42], the authors have applied well-known Weibull probability density function (PDF) for modeling uncertainty of stochastic wind speed to incorporate wind power output into hybrid power systems.

**TABLE 1. Abbreviations.**

| Abbreviation | Methods and terms |
|---|---|
| ABC | Artificial bee colony |
| ACO | Ant colony optimization |
| AGSO | Adaptive group search optimization |
| AMFO | Adaptive moth flame optimization |
| BBSA | Binary backtracking search algorithm |
| BMO | Barnacles mating optimization |
| BSA | Bird swarm algorithm |
| DE | Differential evolution |
| DSA | Differential search algorithm |
| EP | Evolutionary programming |
| FMF-PSO | Fuzzy membership function based PSO |
| GA | Genetic algorithm |
| GABC | Guided artificial bee colony |
| GA-MPC | GA based on multi-parent crossover |
| GWO | Grey wolf optimizer |
| GWSO | Glowworm swarm optimization |
| HSA | Harmony search algorithm |
| IADE | Improved adaptive DE |
| ICBO | Improved colliding bodies optimization |
| IMFO | Improved moth flame optimization |
| ISO | Independent system operator |
| ISSO | Improved social spider optimization |
| MBFA | Modified bacteria foraging algorithm |
| MGO | Modified grasshopper optimization |
| MICA | Modified imperialist competitive algorithm |
| MINLP | Mixed integer nonlinear programming |
| MOEA/D | Multi-objective EA based decomposition |
| MPIO | Modified pigeon-inspired optimization |
| MSA | Moth swarm algorithm |
| OPF | Optimal power flow |
| PDF | Probability density function |
| PEM | Point estimate method |
| PPSO | Phasor PSO |
| PSO | Particle swarm optimization |
| PV | Photovoltaic |
| RESs | Renewable energy sources |
| SFO | Sunflower optimization |
| SHADE | Success history-based adaptation for DE |
| SKH | Stud krill herd |
| SQP | Sequential quadratic programming |
| TG | Thermal generator |
| WF | Windfarm |
| WT | Wind turbine |

In the last decade, some studies also have been documented [43]–[53] to find optimal solution to the OPF problems in the thermal, wind, and solar energy sources-based hybrid power systems. In recent studies [43]–[53], different metaheuristic approaches including grey wolf optimizer (GWO) [43], fuzzy membership function based PSO (FMF-PSO) [44], improved adaptive DE (IADE) [45], modified imperialist competitive algorithm based on sequential quadratic programming (MICA-SQP) [46], modified JAYA [47], hybrid of phasor PSO and GSA [48], barnacles mating optimization (BMO) [49], PSO [50], Hybrid of DE and PSO [51], MBFA [52], and sunflower optimization (SFO) [53] have been proposed for solving the OPF problems in hybrid power systems. In studies [43]–[53], mostly Lognormal PDF and Weibull PDF have been applied for

**TABLE 2.** Summary of studies to optimal solutions to the OPF problems in hybrid power systems.

| | Objectives | | | Energy Sources | | | Uncertainty Models | | |
|---|---|---|---|---|---|---|---|---|---|
| **Algorithm** | $\xi_q$ | $P_{loss}$ | $E_p$ | $Thermal$ | $Wind$ | $Solar$ | $Wind_{speed}$ | $Solar_{irradi}$ | $Utility_{load}$ |
| DE [8] | ✓ | - | ✓ | ✓ | ✓ | ✓ | ✓ | ✓ | - |
| PSO [9] | ✓ | ✓ | - | ✓ | ✓ | ✓ | ✓ | ✓ | - |
| GABC [38] | ✓ | - | ✓ | ✓ | ✓ | - | ✓ | - | - |
| MBFA and GA [39] | ✓ | - | - | ✓ | ✓ | - | ✓ | - | - |
| ACO and MBFA [40] | ✓ | ✓ | - | ✓ | ✓ | - | ✓ | - | - |
| GWSO [41] | ✓ | ✓ | - | ✓ | ✓ | - | ✓ | - | - |
| Self-Adaptive EP [42] | ✓ | - | - | ✓ | ✓ | - | ✓ | - | - |
| GWO [43] | ✓ | - | ✓ | ✓ | ✓ | ✓ | ✓ | ✓ | - |
| FMF-PSO [44] | ✓ | ✓ | ✓ | ✓ | ✓ | ✓ | ✓ | ✓ | - |
| IADE [45] | ✓ | ✓ | ✓ | ✓ | ✓ | ✓ | - | - | - |
| MICA-SQP [46] | ✓ | - | ✓ | ✓ | ✓ | ✓ | ✓ | ✓ | - |
| MJAYA [47] | ✓ | ✓ | ✓ | ✓ | ✓ | ✓ | - | - | - |
| Hybrid PPSO & GSA [48] | ✓ | ✓ | - | ✓ | ✓ | ✓ | ✓ | ✓ | - |
| BMO [49] | ✓ | ✓ | ✓ | ✓ | ✓ | ✓ | ✓ | ✓ | - |
| PSO [50] | ✓ | - | - | ✓ | ✓ | ✓ | ✓ | ✓ | - |
| Hybrid DE & PSO [51] | ✓ | - | ✓ | ✓ | ✓ | ✓ | ✓ | ✓ | - |
| MBFA [52] | ✓ | ✓ | ✓ | ✓ | ✓ | ✓ | ✓ | ✓ | - |
| SFO [53] | ✓ | - | - | ✓ | ✓ | ✓ | - | - | - |

Quadratic fuel cost ($\xi_q$), power loss in transmission lines ($P_{loss}$), emission pollution ($E_p$)

modeling uncertainty of the stochastic solar irradiance and wind speed, respectively.

Table 2 represents the summary of all of the aforementioned studies [38]–[53] have been conducted on thermal and wind or thermal, wind, and solar energy sources-based hybrid power systems. As specified in Table 2, OPF problem primary objective – quadratic fuel cost $\xi_q$ (electricity generation cost) minimization is considered in all studies. Moreover, other objectives such as reducing power loss in transmission lines $P_{loss}$ is considered in 9 studies and emission pollution $E_p$ is considered in 10 studies. It is also observed from Table 2, in most studies the uncertainty of power output from RESs was incorporated for solving the OPF problems in hybrid power systems.

### C. PROBLEM STATEMENT

In study [8], authors have proposed success history-based adaptation differential evolution (SHADE) to find optimal solution to the OPF problems in hybrid power system. The OPF problem objectives - to reduce electricity generation cost and emission pollution are considered. In study [9], the author has proposed a fuzzy logic technique based on PSO finding optimal solution to the multi-objective OPF problems in hybrid power systems, by considering objectives to reduce active power output cost and power loss in transmission lines.

In both studies [8], [9], uncertainty of stochastic solar irradiance and wind speed are incorporated into the power system to solve the OPF problems. However, the utility load demand uncertainty has been ignored in these studies [8], [9]. On the other hand, SHADE and PSO may be inefficient to find optimal solutions to the nonlinear and quadratic OPF problems because DE has a premature convergence property [54] and PSO is incapable of searching neighborhood existing solutions in nonlinear quadratic optimization problems [55].

### D. CONTRIBUTION AND PAPER ORGANIZATION

In study [56], authors have proposed a new bio-inspired bird swarm algorithm (BSA). In which, it has been observed that the BSA has good diversity and can flexibly regulate its four different search strategies such as foraging, vigilance, producer and scrounger to explore the search space. Moreover, BSA can improve its convergence speed without affecting the stability and accuracy of optimal solutions by making better balancing among exploration and exploitation of search space. In fact, under suitable interpretations, DE and PSO mutation operators are distinct forms of the proposed BSA approach. In which, the bird's social behaviour such as the scrounger formula is similar to the DE mutation operator and the foraging formula is similar to the PSO. Moreover, the BSA has prominent distinguishing features, in addition to the merits of the DE and PSO.

In study [56], optimization results have proved the superiority of the BSA as compared to DE and PSO to optimize the Rastrigin function $F_9$, which is a well-known quadratic benchmark function for performance evaluation of optimization algorithms. The primary objective function of the OPF problem is to reduce power generation cost, which follows a quadratic nature function. Inspired by the study [56], we have proposed BSA to find an optimal solution to the OPF problem in the hybrid power system. This research study is an

extension of [57] our conference paper already published. It have following knowledge contribution in academic research;

- A method based on BSA is proposed for finding an optimal solution to the OPF problem in the hybrid power system by incorporating uncertainty of the utility load demand and stochastic power output from RESs.

We have used a modified IEEE-30 bus test system to measure and evaluate the performance BSA for finding an optimal solution tothe OPF problem in the hybrid power system. Simulation based optimization results have shown the superiority of BSA approach to solve the OPF problems (see Table 10 and Figure 8).

The organization of paper is as follows: The uncertainty modeling of utility load demand, stochastic solar irradiance, and wind speed are described in section II. The section III consists of OPF problem formulation, objective function, and different constraints. In section IV, we have explained the proposed metaheuristic method. The simulation-based experiment results for the proposed BSA approach and other algorithms are specified in V and concluding remarks are written in section VI.

## II. UNCERTAINTY MODELLING OF WIND SPEED, SOLAR IRRADIANCE, AND UTILITY LOAD DEMAND

The most significant aspect of uncertainty modeling is to use an appropriate PDF for predicting the values of uncertain or random variables. We have used the Lognormal PDF and Weibull PDF for modeling uncertainty of solar irradiance and stochastic wind speed by adopting same strategy proposed in study [8]. We have utilized the same formula and approach of Gaussian (normal) PDF presented in studies [59], [60] for modeling uncertainty of utility load demand. The Hong's point estimate method (PEM) proposed in study [61] has been used for calculating the utility load demand on load buses.

In this section, first, we have described the model for handling the uncertainty of wind speed to incorporate wind power output. Secondly, we have explained the model for incorporating stochastic solar power in the power system. Lastly, we have described Gaussian PDF for handling uncertainty of utility load demand.

### A. UNCERTAINTY MODELING OF STOCHASTIC WIND SPEED

In the research literature, the well-known Weibull PDF has been mostly applied for modeling the wind speed v (m/s) [38]–[40], [42] to incorporate the stochastic nature wind electricity generation into the power system. The uncertainty modeling stochastic wind speed using Weibull PDF can be defined as:

$$f_v(v) = \left(\frac{v}{c}\right)^{(k-1)} \times \left(\frac{k}{c}\right) \times e^{-(v/c)^k} \quad for \quad 0 < v < \infty, \tag{1}$$

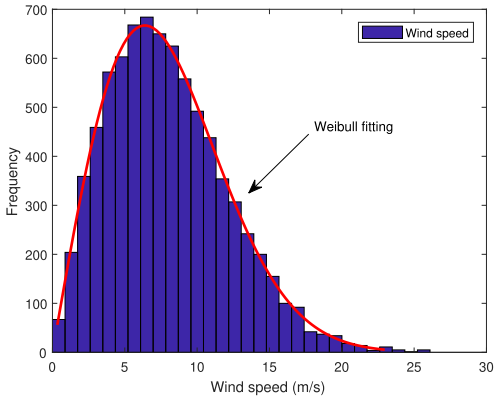


(a) Bus 5

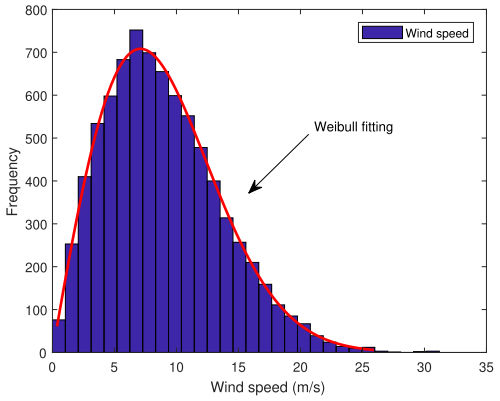


(b) Bus 11

**FIGURE 1.** Weibull fitting of wind speed.

where, scale factor c and shape factor k are parameters and its mean ($M_{wbl}$) can be calculated as:

$$M_{wbl} = c \times \Gamma(1 + k^{-1}), \tag{2}$$

where, $\Gamma()$ represents the gamma function and it can be formulated as:

$$\Gamma(x) = \int_0^\infty e^{-1} t^{x-1} dt. \tag{3}$$

For the performance evaluation of BSA, we have modified standard IEEE-30 bus test system, in which two traditional thermal energy sources at 5 and 11 generator buses are replaced with wind energy sources (windfarms). The total number of wind turbines (WTs) in each windfarm and values of c and k of Weibull PDF parameters are given in Table3. Frequency distributions and Weibull fitting of wind speed of windfarms energy sources attached at buses 5 and 11 are determined after execution of 8000 Monte Carlo simulation scenarios and plotted in Figure 1.

**TABLE 3.** Windfarms and Weibull PDF parameters [8].

| Energy source | WTs | Rated power, $P_{wr}(MW)$ | PDF parameters | Weibull mean, $M_{wbl}$ |
|---|---|---|---|---|
| 1. $WF_5$ | 25 | 75 | c=9 , k=2 | v=7.953 m/s |
| 2. $WF_{11}$ | 20 | 60 | c=10 , k=2 | v=8.892 m/s |

In a windfarm, the actual power output of WT depends upon wind speed v (m/s) it meets. In both windfarms, each WT has a 3 MW rated power output. The cumulative rated power generations of windfarms connected at generator buses 5 and 11 are 75 MW from 25 WTs and 60 MW from 20 WTs, respectively. The WT electricity generation can be formulated as follows [8]:

$$P_w(v) = \begin{cases} P_{wr}, & for \quad v_r < v \le v_{out}, \\ P_{wr} \times \left(\dfrac{v - v_{in}}{v_r - v_{in}}\right), & for \quad v_{in} \le v \le v_r, \\ 0, & for \quad v < v_{in} \quad and \quad v > v_{out}, \end{cases} \tag{4}$$

where, $v_{in}$ is cut-in, $v_{out}$ is cut-out and $v_r$ is cut-in rated wind speed met to WT and its rated power output is represented as $P_{wr}$. We have considered $v_r = 16$ m/s, $v_{out} = 25$ m/s, and $v_{in} = 3$ m/s for wind power output calculation purpose.

The histograms in Figure 2 indicate wind power output based on wind speed Weibull distribution plotted in Figure 1, from windfarms connected at bus 5 and bus 11. It is observed from WT power output Eq. 4 that WT provides rated power output $P_{wr}$ when wind speed is in range [$v_r$ $v_{out}$]. The wind power output is calculated as [8]:

$$f_w(P_w)_{\{P_w = P_{wr}\}} = e^{-\left(\frac{v_r}{c}\right)^k} - e^{-\left(\frac{v_{out}}{c}\right)^k}. \tag{5}$$

The WT provides wind power in continuous form when wind speed is in range [$v_{in}$ $v_r$] and wind power output for this region is measured as [8]:

$$f_w(P_w) = \frac{k(v_r - v_{in})}{c^k \times P_{wr}} \times \left\{v_{in} + \frac{P_w}{P_{wr}}(v_r - v_{in})\right\}^{k-1} \times e^{-\left\{\frac{v_{in} + \frac{P_w}{P_{wr}}(v_r - v_{in})}{c}\right\}^k}. \tag{6}$$

The electricity generation is zero when wind speed is not in range [$v_{in}$ $v_{out}$].

$$f_w(P_w)_{\{P_w = 0\}} = 1 - e^{-\left(\frac{v_{in}}{c}\right)^k} + e^{-\left(\frac{v_{out}}{c}\right)^k}, \tag{7}$$

### B. UNCERTAINTY MODELING OF SOLAR IRRADIANCE

The probabilistic model for solar irradiance I ($W/m^2$) follows lognormal PDF and it is generally utilized for handling the stochastic solar power generation in hybrid power systems [58]. The uncertainty of solar irradiance I ($W/m^2$) mathematically can be written as [58]:

$$f_I(I) = \frac{1}{I\sigma\sqrt{2\pi}} \times e^{\left\{\frac{-(lnI - \mu)^2}{2\sigma^2}\right\}} \quad for \quad I > 0, \tag{8}$$

where $\mu$ in mean of solar irradiance and $\sigma$ is standard deviation of solar irradiance. Lognormal PDF mean ($M_{lgn}$) is defined as:

$$M_{lgn} = e^{\left(\mu + \frac{\sigma^2}{2}\right)}. \tag{9}$$

Assumed values for mean ($\mu$) of solar irradiance and standard deviation ($\sigma$) have been specified in Table 4. In a modified IEEE-30 bus test system, we have replaced two thermal

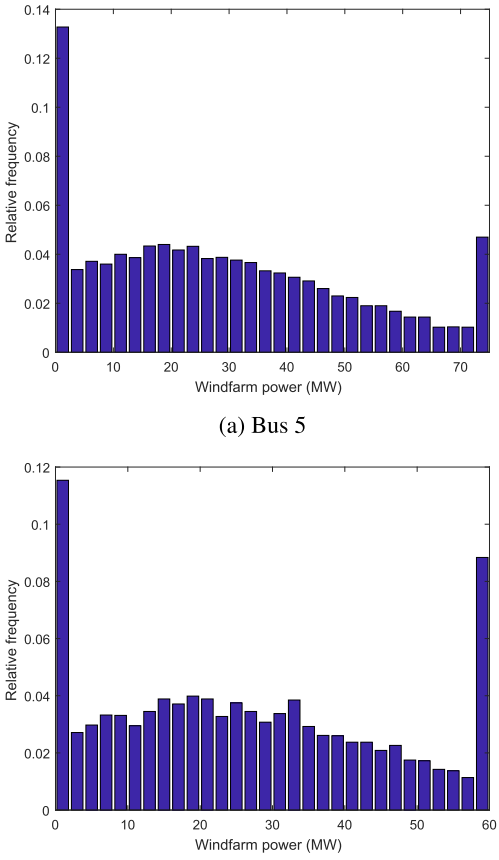


(a) Bus 5




(b) Bus 11

**FIGURE 2.** Windfarm power output.

**TABLE 4.** Solar PV units and Lognormal PDF parameters [8].

| Energy source | Rated power, $P_{pvr}(MW)$ | Lognormal PDF parameters | Lognormal mean, $M_{lgn}$ |
|---|---|---|---|
| 1. $SPV_8$ | 35 | $\mu = 6\,, \sigma = 0.6$ | $I = 485\,W/m^2$ |
| 2. $SPV_{13}$ | 50 | $\mu = 6\,, \sigma = 0.6$ | $I = 485\,W/m^2$ |

energy sources connected at 8 and 13 buses with two solar PV units. The lognormal PDF fitting and solar irradiance frequency distributions for solar energy sources connected at 8 and 13 buses are achieved after executing simulation of 8000 Monte Carlo scenarios, which are plotted in Figure 3. The solar PV unit available or actual solar power generation subject to solar irradiance I ($W/m^2$) and solar PV unit electricity generation modeled as [8]:

$$P_{pv}(I) = \begin{cases} P_{pvr} \times \left(\dfrac{I}{I_{std}}\right), & for \quad I \ge I_c, \\ P_{pvr} \times \left(\dfrac{I^2}{I_{std} \times I_c}\right), & for \quad 0 < I < I_c, \end{cases} \tag{10}$$

where $I_{std}$ and $I_c$ indicate the solar irradiance and certain solar irradiance point in a standard environment, respectively. The solar PV unit rated power output is represented as $P_{pvr}$.

In this study, we assumed $I_{std} = 800\ W/m^2$ and $I_c = 120\ W/m^2$. The rated power outputs related to solar PV units that are connected at generator bus 8 and 13 are

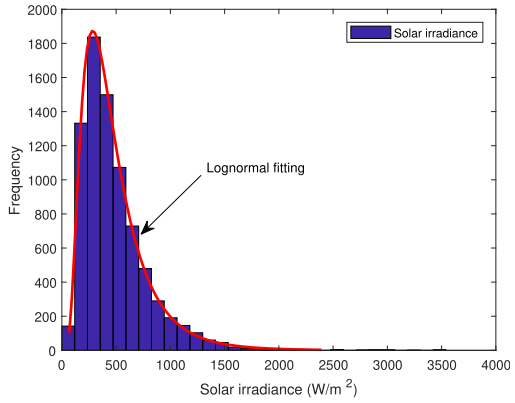


(a) Bus 8

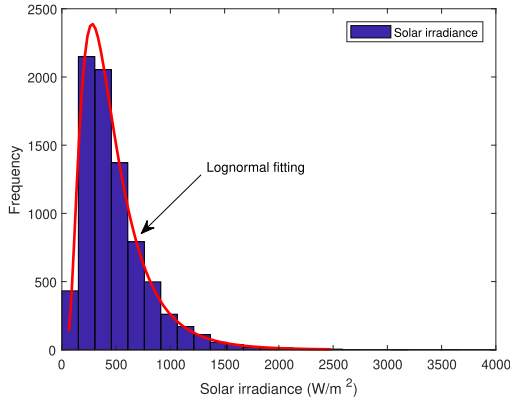


(b) Bus 13

**FIGURE 3.** Lognormal fitting of solar irradiance.

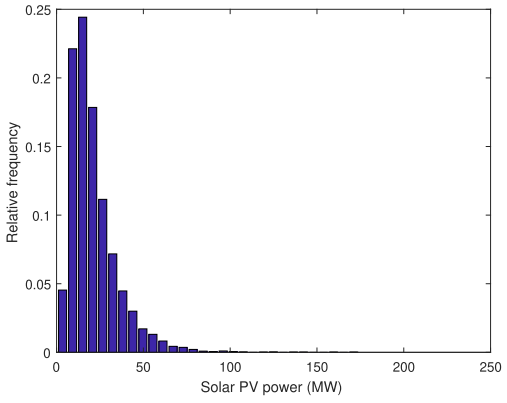


(a) Bus 8

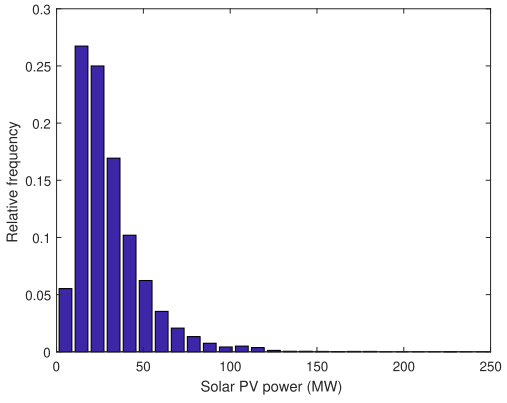


(b) Bus 13

**FIGURE 4.** Power output from solar PV units.

$P_{pvr} = 35$ MW and $P_{pvr} = 50$ MW, respectively. The histograms in Figure 4 represent the stochastic solar power output based on solar irradiance I $(W/m^2)$ distribution shown in Figure 3, from solar PV units.

### C. UTILITY LOAD DEMAND UNCERTAINTY MODELING

The utility load demand is also stochastic due to variation in consumers' load demand that directly affects spinning reserve cost in a power system. Therefore, modeling the utility load demand uncertainty has a significant impact on solving the OPF problem and achieving accuracy in planning and operations of the power system. In this study, utility active (real) load is considered as a random variable and power factor is considered as constant. According to the constant power factor, the change in reactive power of each load bus or PQ bus depends upon its active load in the power system. We have used a Gaussian PDF [59], [60] to model the uncertainty of utility load demand on each load bus in transmission system.

The prediction of load demand on a load bus follows Gaussian PDF as:

$$f(P_{d,i}) = \frac{1}{\sqrt{(2\pi)\sigma_i}} \times e^{\left\{-\frac{(P_{d,i}-\mu_i)^2}{2\sigma_i^2}\right\}}, \tag{11}$$

where, $P_{d,i}$ is active load demand, $\sigma_i$ is standard deviation and $\mu_i$ is mean value of active load at $i^{th}$ load bus.

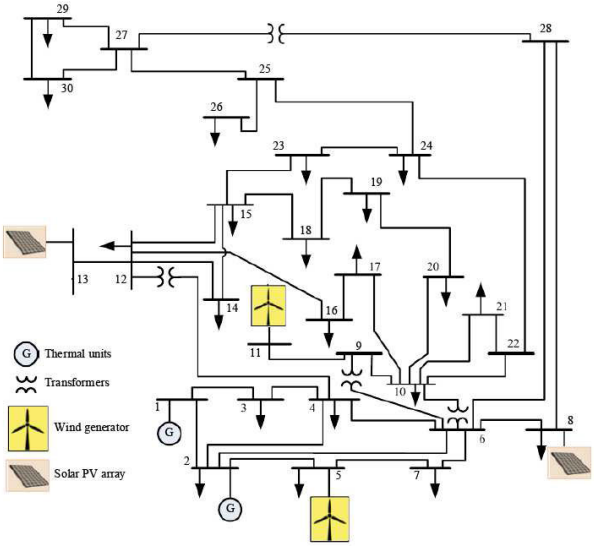


**FIGURE 5.** Modified IEEE-30 bus test system.

We have utilized modified IEEE-30 bus system for performance evaluation of our proposed method, in which four thermal energy sources at 5, 8, 11, and 13 generator buses are replaced with RESs due to emission pollution and global

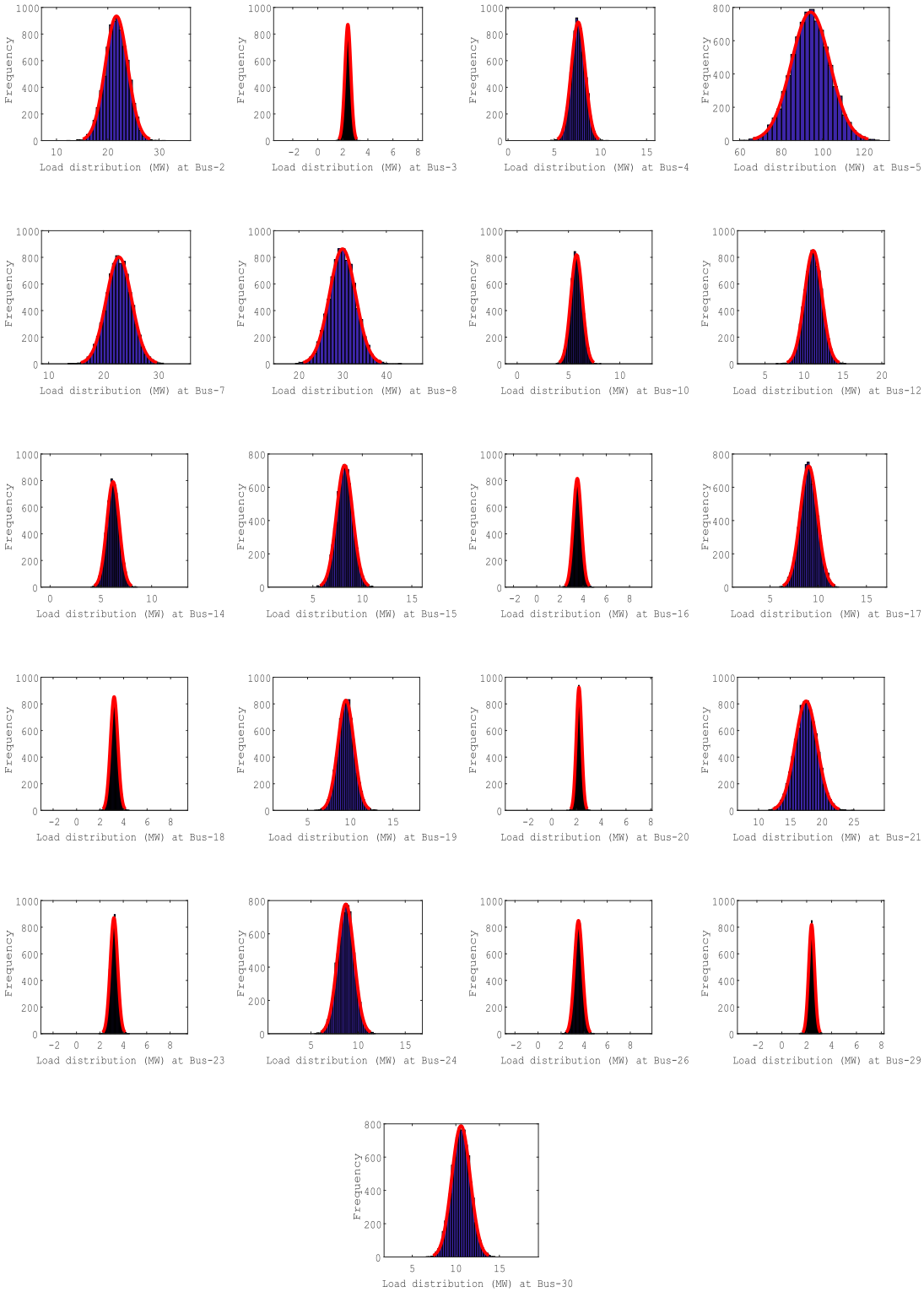


**FIGURE 6.** Gaussian distribution of utility load demand on load or PQ buses.

warming issues. The down-arrow (↓) symbol represents load or PQ bus shown in Figure 5. The active (real) load demand mean value $\mu$ has been considered equal to the base active load of each load bus, and 10% of the mean value $\mu$ has been considered as standard deviations $\sigma$ of active load on each load bus for modeling uncertainty of utility active load

demand across the modified IEEE-30 bus test system. Plotted histograms in Figure 6 based on Gaussian PDF and represent the distribution of active load demands on load or PQ buses, which are achieved after execution of 8000 Monte-Carlo simulation scenarios.

In the research literature, many approximation methods based on the analytical approach have been documented [62] for handling the uncertainty in power systems. The common uncertain source method, the discretization method, the truncated Taylor series expansion method, and the point estimate method are examples of these methods. Some of the analytical approximation methods follow the uncertain or random variable's PDF. In 1998, H.P. Hong [61] developed an efficient PEM to measure the moments of Z = h(x), where Z represents an uncertain or random quantity and it is a function of n uncertain variables. The PEM is a simple to use method for measuring the moments Z and does not require derivatives of h(x) or any iteration as compared to other approximation methods such as the discretization method and Taylor series expansion method. The PEM can be utilized directly with a deterministic computer program. Based on the above facts, we used Hong's PEM for calculating the approximate load on load buses.

Hong's PEM concentrates upon statistical information obtained through initial few moments of a random variable on m concentrations for every variable. In which $m \times n$ points concentration matching is considered to achieve first non-crossed moments ($m \times n$) and crossed second-order moments of each uncertain variable. The simplest case of Hong's PEM is the 2m scheme, in which skewness of an uncertain variable's PDF and correlation between the uncertain variables are considered for predicting the value of random quantity. Another particular case of Hong's PEM is the 2m +1 scheme, in addition to the skewness of the uncertain variable's PDF and correlation between the uncertain variables, kurtosis of the uncertain variable's PDF is also considered in this scheme to calculate the random quantity. More detail of Hong's PEM is available in [61]–[63].

**TABLE 5.** Deterministic utility load on load buses.

| | | | Deterministic load demand (MW) | |
|---|---|---|---|---|
| Load bus | Mean($\mu$) | Standard deviation($\sigma$) | 2m scheme | 2m+1 scheme |
| 2 | 21.7 | 2.17 | 23.87 | 23.87 |
| 3 | 2.4 | 0.24 | 2.64 | 2.64 |
| 4 | 7.6 | 0.76 | 8.34 | 8.34 |
| 5 | 94.2 | 9.42 | 103.54 | 103.54 |
| 7 | 22.8 | 2.28 | 25.10 | 25.10 |
| 8 | 30 | 3.0 | 32.92 | 32.92 |
| 10 | 5.8 | 0.58 | 6.38 | 6.38 |
| 12 | 11.2 | 1.12 | 12.37 | 12.37 |
| 14 | 6.2 | 0.62 | 6.75 | 6.75 |
| 15 | 8.2 | 0.82 | 9.05 | 9.05 |
| 16 | 3.5 | 0.35 | 3.80 | 3.80 |
| 17 | 9 | 0.9 | 9.92 | 9.92 |
| 18 | 3.2 | 0.32 | 3.55 | 3.55 |
| 19 | 9.5 | 0.95 | 10.47 | 10.47 |
| 20 | 2.2 | 0.22 | 2.47 | 2.47 |
| 21 | 17.5 | 1.75 | 19.24 | 19.24 |
| 23 | 3.2 | 0.32 | 3.50 | 3.50 |
| 24 | 8.7 | 0.87 | 9.54 | 9.54 |
| 26 | 3.5 | 0.35 | 3.83 | 3.83 |
| 29 | 2.4 | 0.24 | 2.65 | 2.65 |
| 30 | 10.6 | 1.06 | 11.7 | 11.7 |

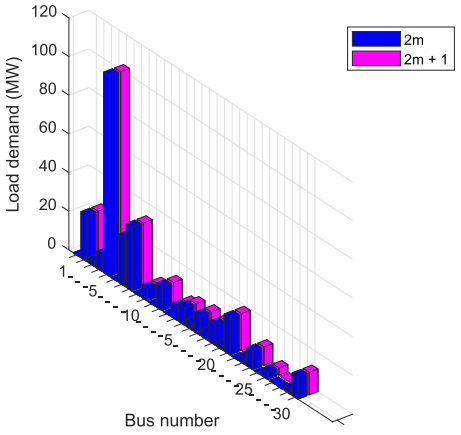


**FIGURE 7.** Utility load demnd on load buses.

In this research work, we have utilized Hong's PEM [61] by taking Gaussian PDFs of active load demands on modified IEEE-30 bus test system load or PQ buses as input from plotted histograms in Figure 6, to calculate active load on each bus. The deterministic load on each load bus obtained from using particular schemes of Hong's PEM such as 2m and 2m+1 is specified in Table 5 and plotted in Figure 7. The deterministic active load demand on each load bus based on both 2m and 2m+1 schemes is similar. Therefore, we have used the simplest 2m scheme of Hong's PEM for calculating load demand on each load bus to find an optimal solution to the OPF problem in the hybrid power system.

## III. THE OPF PROBLEM FORMULATION

The OPF in the traditional thermal energy sources-based power system is a quadratic nature nonconvex and nonlinear problem, in which stable and secure settings of operating points in electricity generation plants are obtained for minimizing certain objectives. The OPF problem objective written as [45]:

$$\begin{aligned} &\textit{Minimize}: \quad f(x,u) \\ &s.t.: \quad g(x,u) = 0 \\ &\qquad\quad h(x,u) \leq 0, \end{aligned} \tag{12}$$

where, u is a set of control variables and x is a set of state variables. The function $f(x,u)$ represents the objective of the OPF problem. The function $g(x,u)$ represents equality constraints and $h(x,u)$ represents inequality constraints.

The power flow in system is controlled by control or independent variables, while state variables described power system state. The control variables consist of all bus generators active power excluding slack (swing) bus active power, all generators or energy sources voltage magnitudes, shunt compensator at selected buses, and transformer tap in power system network. The state variables consist of generators' reactive power, swing bus active power output, line loading of transmission lines, and voltages magnitude at load buses.

### A. CONSTRAINTS

Balancing both active (real) power and reactive power follow equality constraints, while security constraints and equipment's operating limits of transmission lines and load buses follow inequality constraints. The description of both types of constraints is provided herein.

#### 1) EQUALITY CONSTRAINTS

In a power system, active (real) power generation from energy sources must be equal to active (real) load demands and power loss in transmission lines. Similarly, reactive power output from all energy sources also must be equal to demand and loss of reactive power. In the power system, equality constraints can be written as according to study [45]:

$$P_{Gi} - P_{Di} = V_i \sum_{j=1}^{NB} V_j \left\{ G_{ij} cos(\theta_{ij}) + B_{ij} sin(\theta_{ij}) \right\} \quad \forall\, i \in NB \tag{13}$$

$$Q_{Gi} - Q_{Di} = V_i \sum_{j=1}^{NB} V_j \left\{ G_{ij} sin(\theta_{ij}) - B_{ij} cos(\theta_{ij}) \right\} \quad \forall\, i \in NB \tag{14}$$

where, the term $P_{Gi}$ indicates the active power and term $Q_{Gi}$ represents reactive power generation from energy source attached at $i^{th}$ bus. The term $P_{Di}$ represents the load demand of active power and term $Q_{Di}$ is demand of reactive power at $i^{th}$ load bus. The term $V_i$ represents $i^{th}$ bus voltage magnitude, while term $V_j$ represents $j^{th}$ bus voltage magnitude. The term $\theta_{ij} = \theta_i - \theta_j$ shows difference of voltage angles $\theta_i$ and $\theta_j$ at $i^{th}$ and $j^{th}$ buses. The term $G_{ij}$ is transfer conductance and $B_{ij}$ is transfer susceptance in $i^{th}$ and $j^{th}$ buses.

#### 2) INEQUALITY CONSTRAINTS

In power systems, load buses and transmission lines security constraints, secure and stable equipment's physical settings, and equipment's operating lower and upper limits are considered as inequality constraints. These are mathematically described as follows [45]:

$$P_{TG_i}^{min} \le P_{TG_i} \le P_{TG_i}^{max} \qquad i = 1, \ldots, N_{TG}, \tag{15}$$

$$P_{ws,j}^{min} \le P_{ws,j} \le P_{ws,j}^{max} \qquad j = 1, \ldots, N_{WF}, \tag{16}$$

$$P_{pvs,k}^{min} \le P_{pvs,k} \le P_{pvs,k}^{max} \qquad k = 1, \ldots, N_{PV}, \tag{17}$$

$$Q_{TG_i}^{min} \le Q_{TG_i} \le Q_{TG_i}^{max} \qquad i = 1, \ldots, N_{TG}, \tag{18}$$

$$Q_{ws,j}^{min} \le Q_{ws,j} \le Q_{ws,j}^{max} \qquad j = 1, \ldots, N_{WF}, \tag{19}$$

$$Q_{pvs,k}^{min} \le Q_{pvs,k} \le Q_{pvs,k}^{max} \qquad k = 1, \ldots, N_{PV}, \tag{20}$$

$$V_{Gi}^{min} \le V_{Gi} \le V_{Gi}^{max} \qquad i = 1, \ldots, NG, \tag{21}$$

$$V_{L_p}^{min} \le V_{L_p} \le V_{L_p}^{max} \qquad p = 1, \ldots, NL. \tag{22}$$

The active (real) power output boundary limits of traditional thermal energy source and RESs such as windfarms and solar PV units are represented in constraints (15)-(17) and $N_{TG}$, $N_{WF}$ and $N_{PV}$ are total number of traditional thermal energy sources, windfarms, solar PV units, respectively. The reactive power output boundary limits of all energy sources or generators including traditional thermal energy sources, windfarms, and solar PV units are defined by constraints (18)-(20), respectively. On load buses and generator buses voltage magnitude boundary limits are defined by constraint (21) and (22), respectively. $NG$ is number of generator buses. In each inequality constraints max and min superscripts show boundary limits of the corresponding parameter. $NL$ is number of load buses.

### B. OBJECTIVE FUNCTION

To reduce electricity generation cost from traditional thermal energy sources and RESs and including emission cost (e.g., carbon tax) is our objective for finding an optimal solution to the OPF problem in the hybrid power system. The minimization of electricity output cost objective is stated as follows:

$$Minimize \quad \xi = \xi_T(P_{TG}) + \sum_{j=1}^{N_{WF}} \xi_{w,j}(P_{w,j}) + \sum_{k=1}^{N_{PV}} \xi_{pv,k}(P_{pv,k}) + \xi_E. \tag{23}$$

The first term $\xi_T(P_{TG})$ represents power generation cost of thermal energy sources, which based on valve-point loading effects quadratic curve. The second term $\sum_{j=1}^{N_{WF}} \xi_{w,j}(P_{w,j})$ represents the cost of power output from windfarms. In objective function, the third term $\sum_{k=1}^{N_{PV}} \xi_{pv,k}(P_{pv,k})$ is cost of solar power output from solar PV units. The last term $\xi_E$ is the cost of emission (e.g., carbon tax). The detailed modeling of traditional thermal and RESs power generation cost functions and emission cost are provided herein.

#### 1) THERMAL POWER COST CURVE

The traditional thermal energy source required fossil fuel to produce electricity. The power generation cost of fossil fuel based energy sources can be calculated by regular quadratic fuel curve, valve-point effects quadratic fuel curve, and piecewise quadratic fuel curve [38]. In some practical cases, thermal power is generated from traditional thermal energy sources using different fossil fuels like natural gases,coal and oil. The power output cost from these types of energy sources is calculated using the piecewise quadratic fuel cost curve.

In this study, we assumed that the same fossil fuel based traditional thermal energy sources are used for power generation purposes. Therefore, to calculate the power cost related to thermal energy source, we used two forms of fuel cost curve; 1) quadratic fuel curve and 2) valve-point effects quadratic fuel curve. The generated power (MW) from thermal energy source followed a quadratic relationship with fossil fuel cost ($/h) as [45]:

$$\xi_{T_0}(P_{TG}) = \sum_{i=1}^{N_{TG}} a_i + b_i P_{TG_i} + c_i P_{TG_i}^2, \tag{24}$$

where, $P_{TG_i}$ is $i^{th}$ thermal energy source power output. $a_i$, $b_i$, and $c_i$ are $i^{th}$ thermal energy source cost coefficients.

In a traditional thermal energy source-based power system, the objective function is modeled using valve-point loading effects quadratic fuel cost curve for more precise and realistic measuring of thermal power cost. Because traditional thermal energy source's steam turbines have multi-valve, in such case a variation befall in fuel cost curve. In such case, the fossil fuel cost curve of thermal energy source is measured using valve-point loading effects quadratic fuel cost curve as follows [45]:

$$\xi_T(P_{TG}) = \sum_{i=1}^{N_{TG}} a_i + b_i P_{TG_i} + c_i P_{TG_i}^2 + \left| d_i \times sin\left\{ e_i \times (P_{TG_i}^{min} - P_{TG_i}) \right\} \right|, \quad (25)$$

where, coefficients $d_i$ and $e_i$ represent the valve-point loading effect of $i^{th}$ TG. $P_{TG_i}^{min}$ represents the minimum power output of $i^{th}$ TG during operation. For this study, cost coefficient values of fuel cost curve and valve-point loading effects related to $TG_1$ and $TG_2$ are specified in Table 6.

**TABLE 6. Thermal power emission and cost coefficients [6].**

| **Emission** | | | | | | |
|---|---|---|---|---|---|---|
| Energy source | Bus no. | $\alpha$ | $\beta$ | $\gamma$ | $\omega$ | $\mu$ |
| $TG_1$ | 1 | 4.091 | -5.554 | 6.49 | 0.0002 | 6.667 |
| $TG_2$ | 2 | 2.543 | -6.047 | 5.638 | 0.0005 | 3.333 |
| **Cost** | | | | | | |
| Energy source | Bus no. | a | b | c | d | e |
| $TG_1$ | 1 | 0 | 2 | 0.00375 | 18 | 0.037 |
| $TG_2$ | 2 | 0 | 1.75 | 0.0175 | 16 | 0.038 |

### 2) WIND POWER COST FUNCTION

We have assumed that private parties hold RESs such as solar PV units and windfarms and ISO purchases scheduled power from private parties according to the signed agreement. The wind power cost follows directly proportional relationship to wind-scheduled power and can be formulated as:

$$\lambda_{ws,j}(P_{ws,j}) = g_j P_{ws,j}, \quad (26)$$

where, $\lambda_{ws,j}$ is a function to calculate power cost of wind-scheduled power $P_{ws,j}$ received from $j^{th}$ windfarm and $g_j$ is cost coefficient of wind-scheduled power related to $j^{th}$ windfarm.

The distributions of windfarms power output are shown in Figure 2. The available power from windfarms can be less or more than wind-scheduled power because of fluctuant and stochastic wind power output. In an overestimation scenario, when wind power supplied by windfarms operators is less than the wind-scheduled power, the ISO is required to have a spinning reserve based on utility load demand. The wind power reserve cost $\lambda_{wr,j}$ for $j^{th}$ windfarm can be calculated as [39]:

$$\lambda_{wr,j}(P_{ws,j} - P_{wav,j}) = K_{wr,j} \int_0^{P_{ws,j}} \left(P_{ws,j} - P_{w,j}\right) \times f_w\left(P_{w,j}\right) dP_{w,j}, \quad (27)$$

where, $P_{wav,j}$, $K_{wr,j}$, and $f_w(P_{w,j})$ represent available wind power, coefficient of windfarm reserve cost, and wind power for $j^{th}$ windfarm, respectively.

In a scenario, when wind power supplied by windfarms operator is greater than the wind-scheduled power, if it not possible to reduce power generation from thermal energy sources, the windfarms surplus electricity is dumped and ISO bears penalty cost. The penalty cost $\lambda_{wp,j}$ related to $j^{th}$ windfarm can be formulated as [39]:

$$\lambda_{wp,j}(P_{wav,j} - P_{ws,j}) = K_{wp,j} \int_{P_{ws,j}}^{P_{wr,j}} \left(P_{w,j} - P_{ws,j}\right) \times f_w\left(P_{w,j}\right) dP_{w,j}, \quad (28)$$

where, $K_{wp,j}$ is penalty cost coefficient of $j^{th}$ windfarm.

The cost related to any windfarm power is calculated by adding penalty cost, reserve cost, and its wind-scheduled power cost. The cost coefficients and wind-scheduled power are specified in Table 7. The total wind power cost $\xi_{w,j}(P_{w,j})$ for $j^{th}$ windfarm can be calculated by adding wind-scheduled power cost and both penalty and reserve costs as [39]:

$$\xi_{w,j}(P_{w,j}) = \lambda_{ws,j}(P_{ws,j}) + \lambda_{wr,j}(P_{ws,j} - P_{wav,j}) + \lambda_{wp,j}(P_{wav,j} - P_{ws,j}). \quad (29)$$

**TABLE 7. Cost coefficients and wind-scheduled power.**

| Energy source | Scheduled power (MW) | Scheduled cost coefficient | Penalty cost coefficient | Reserve cost coefficient |
|---|---|---|---|---|
| $WF_5$ | $P_{ws,1}$ = [0 75] | $g_1$=1.6 | $K_{wp,1}$=1.5 | $K_{wr,1}$=3 |
| $WF_{11}$ | $P_{ws,2}$ = [0 60] | $g_2$=1.75 | $K_{wp,2}$=1.5 | $K_{wr,2}$=3 |

### 3) SOLAR POWER COST FUNCTION

Solar power cost is also directly proportional to solar-scheduled power. The solar-scheduled power cost $\lambda_{pvs,k}$ is a function of scheduled power provided from $k^{th}$ solar PV unit, as follows [42]:

$$\lambda_{pvs,k}(P_{pvs,k}) = h_k P_{pvs,k}, \quad (30)$$

where, scheduled power cost coefficient $h_k$ is related to $k^{th}$ solar PV unit and $P_{pvs,k}$ is delivered solar-scheduled power from $k^{th}$ solar PV unit.

In Figure 4, the distributions of power generation from solar PV units are plotted. Similar to the windfarms power output behaviour, in the underestimation scenario, the available power from solar PV units can be more than solar-scheduled power and in an overestimation scenario, the available solar power can be less than solar-scheduled power. In such a case, the ISO requires a spinning reserve energy source. According to the concept presented in the study [42], we have modeled solar reserve cost $\lambda_{pvr,k}$ of $k^{th}$ solar PV unit power output, for an overestimation scenario. It can be formulated as [42]:

$$\lambda_{pvr,k}(P_{pvs,k} - P_{pva,k}) = K_{pvr,k} \times f_{pv}(P_{pva,k} < P_{pvs,k}) \times \left\{ P_{pvs,k} - E(P_{pva,k}, < P_{pvs,k}) \right\}, \quad (31)$$

where, $K_{pvr,k}$ represents coefficient of reserve cost of $k^{th}$ solar PV unit, $P_{pva,k}$ is actual available power received by $k^{th}$ solar PV unit, and $f_{pv}(P_{pva,k} < P_{pvs,k})$ represents the calculation of overestimation scenario related to $k^{th}$ solar PV unit. $E(P_{pva,k} < P_{pvs,k})$ represents the prediction (expectation) of power output from solar PV unit $k^{th}$ below solar-scheduled power $P_{pvs,k}$.

For underestimation scenario, the penalty cost $\lambda_{pvp,k}$ related to $k^{th}$ solar PV unit power output can be formulated as [42]:

$$\lambda_{pvp,k}(P_{pva,k} - P_{pvs,k}) = K_{pvp,k} \times f_{pv}(P_{pva,k} > P_{pvs,k}) \times \{E(P_{pva,k} > P_{pvs,k}) - P_{pvs,k}\}, \quad (32)$$

where, $K_{pvp,k}$ represents the penalty cost coefficient for $k^{th}$ solar PV unit. $f_{pv}(P_{pva,k} > P_{pvs,k})$ represents the calculation of underestimation scenarios related to $k^{th}$ solar PV unit. $E(P_{pva,k} > P_{pvs,k})$ represents the prediction (expectation) of power output from solar PV unit $k^{th}$ above solar-scheduled power $P_{pvs,k}$.

Similar to windfarm power cost, the cost related to a solar PV unit power is calculated by adding penalty cost, reserve cost, and solar-scheduled power cost. The cost coefficients and solar-scheduled power related to solar PV units are specified in Table 8. The total solar power cost $\xi_{pv,k}(P_{pv,k})$ for $k^{th}$ solar PV unit by adding solar-scheduled power cost and both penalty and reserve cost can be measured as [42]:

$$\xi_{pv,k}(P_{pv,k}) = \lambda_{pvs,k}(P_{pvs,k}) + \lambda_{pvr,k}(P_{pvs,k} - P_{pva,k}) + \lambda_{pvp,k}(P_{pva,k} - P_{pvs,k}). \quad (33)$$

**TABLE 8.** Cost coefficients and solar-scheduled power.

| Energy source | Scheduled power (MW) | Scheduled cost coefficient | Penalty cost coefficient | Reserve cost coefficient |
|---|---|---|---|---|
| $SPV_8$ | $P_{pvs,1}$ = [0 35] | $h_1$=1.6 | $K_{pvp,1}$=1.5 | $K_{pvr,1}$=3 |
| $SPV_{13}$ | $P_{pvs,2}$ = [0 50] | $h_2$=1.6 | $K_{pvp,2}$=1.5 | $K_{pvr,2}$=3 |

#### 4) EMISSION COST

The combustion of fossil fuels in traditional thermal sources of energy is the core cause of greenhouse/harmful gases including $SO_x$, $CO_x$, and $NO_x$ emission into the environment. With growing global environmental concerns, to regulate the power system for accounting the minimum emissions is necessary. The total emission $E$ (ton/h) into the environment by a traditional thermal energy source can be formulated as follows [6]:

$$E = \sum_{i=1}^{N_{TG}} \left\{ \left(\alpha_i + \beta_i P_{TG_i} + \gamma_i P_{TG_i}^2\right) \times 0.01 + \omega_i \times e^{(\mu_i P_{TG_i})} \right\}, \quad (34)$$

where, emission coefficient for $i^{th}$ TG are $\alpha_i$, $\beta_i$, $\gamma_i$, $\omega_i$, and $\mu_i$ and values of these coefficient related to $TG_1$ and $TG_2$ are listed in Table 6.

In the recent decade, due to global environmental issues, many countries are imposing a carbon tax to minimize carbon emission into the environment. Therefore, carbon tax widely has been applied to curb greenhouse gases and encourage investment in clean forms of energy, [59]. Carbon tax ($C_{tax}$) imposed on emitted greenhouse gases and emission cost ($/ton) can be calculated as:

$$Emission\ cost, \quad \xi_E = C_{tax} E. \quad (35)$$

**Algorithm 1:** Pseudocode of Proposed Method

```
Input: d: Dimension of problem or vector of control variables X_max = [x^1_max, x^2_max, ..., x^d_max] and X_min = [x^1_min, x^2_min, ..., x^d_min], N: Population size or birds (uniformly distribution ∈ [X_max, X_min])
M: Generations, P ∈ [0.8, 1]: The foraging probability, FQ=10: Frequency of bird's flight, FL ∈ [0.5, 0.9]: Followed coefficient, C = S= 1.5, a1 = a2 =1: Constant parameters and ε: Smallest constant value
Define the itr=0 (iteration variables), related parameters and fitness value for evaluation of objective function, and finding an optimal solution
while (itr < M) do
    if (itr mod FQ ≠ 0) then
        for i=1 to N do
            if P > rand(0, 1) then
                Individual bird in swarm switch into foraging behaviour to explore food patches (Eq. 36)
            else
                Otherwise bird switch int vigilance behaviour(Eq. 37)
            end
        end
    else
        Based on their food reserves birds often switched into producer birds and scrounger birds, after arrived on new site.
        for i=1 to N do
            if i^th bird is a producer then
                i^th bird explore the search space for food patches (Eq. 40)
            else
                Scrounging for hunting food patches (Eq. 41)
            end
        end
    end
    The evaluation of new solutions vector or population
    Greedy approach is applied by comparing the new solutions vector (population) and previous solutions vector
    Search for global optimal
    itr= itr+1.
end
Output: An optimal solution in the new solutions vector (population)
```

## IV. PROPOSED APPROACH TO SOLVE THE OPF PROBLEM

Various nature-inspired metaheuristic algorithms have been developed as a substitute to the mathematical methods for solving optimization problems, in research literature. Population-based BSA [56] is a new stochastic swarm intelligence algorithm. To address the optimization problems, intelligence of bird swarms extracted from bird's social behaviours has been utilized. The birds in the swarm improve their fitness through social behaviours and interactions with other birds in the swarm. The working model of BSA is based on three types of bird behaviours such as foraging, vigilance, and flight behaviour. The BSA can flexibly regulate its four different search strategies such as foraging, vigilance, producer, and scrounger to explore the search space. Based on these facts, the BSA can improve its convergence speed through better balancing between exploitation and exploration of search space without affecting the stability and accuracy of the optimal solution. Therefore, the proposed method based on BSA may provide a more stable and accurate solution for the OPF problems in the hybrid power system. A bird's social behaviours and interactions with other birds in the swarm can be made understand based on well-defined rules as follows:

**Rule 1:** Individual birds in a swarm may switch into two types of behaviours; 1) foraging behaviour and 2) vigilance behaviour, on the basis of the random or stochastic decision.

**Rule 2:** In a swarm, the individual bird may update or improve fitness through social behaviour and by promptly recording self and swarm's best memory or previous experience to explore the food patches in a specific area during foraging behaviour. The best-recorded experience or memory about searching food items can be utilized to explore food patches, and social behaviour and information are shared immediately.

**Rule 3:** On the basis of the bird's vigilance behaviour, an individual bird wishes travel to the swarm's center. The competition between birds' movement towards the center of the swarm may affect the individual bird's struggle to reach the center of the swarm. The probability of a bird near a swarm's center based on birds' food reserves and a bird having greater food reserves than other birds will be at the swarm's center.

**Rule 4:** The birds in a swarm have flight behaviour due to foraging behaviour or any other reason. During the flight behaviour the birds in the swarm can be often switched again into two types of birds; 1) producer birds and scrounger birds on the basis of their food reserves. Birds that have food reserved between lowest and highest are randomly switched into scrounger and producer.

**Rule 5:** After arrival at a new place, birds divide into producers and scroungers. The producers search food items or patches and randomly followed by scroungers to search food patches.

Precise pseudo code of proposed method based on above defined rules of BSA is given in Algorithm 1. Three types of bird's behaviours such as vigilance behaviour, foraging behaviour, and flight behaviour are briefly described here.

### A. FORAGING BEHAVIOUR

Stochastic decision (Rule 1) is taken according to the probability P of bird foraging food. Individual birds in swarms switched into foraging behaviours if probability P is greater than randomly selected constant value from a uniform normal distribution (0,1), otherwise the bird has vigilance behaviour. The best recorded experience or memory about searching food items can be utilized to explore food patches, and social behaviour and information are shared immediately (Rule 2). It can be mathematically modeled as [56]:

$$x_{i,j}^{t+1} = x_{i,j}^{t} + \left(p_{i,j} - x_{i,j}^{t}\right) \times C \times rand(0,1) + \left(g_j - x_{i,j}^{t}\right) \times S \times rand(0,1), \quad (36)$$

where, C represents cognitive and S represents social accelerated positive coefficients. $p_{i,j}$ represents the past best position (local optimal) of $i^{th}$ bird, while $g_j$ is the swarm shared best (global optimal) past position. The function rand(0,1) represents uniform distribution of numbers in (0, 1). The term $x_{i,j}^{t}\,(i \in \{1, 2, \ldots, N\})$ represents N virtual birds' position at time t, having vigilance or foraging behaviour and term $(j \in \{1, 2, \ldots, D\})$ represents dimensions of available search space in which birds take flight.

### B. VIGILANCE BEHAVIOUR

According to Rule 3, birds would not travel directly towards the swarm's center. However, individual birds may struggle to travel towards the swarm's center and birds' movement may be affected by competition with each other. Individual bird's movement or vigilance behavior modeled as [56]:

$$x_{i,j}^{t+1} = x_{i,j}^{t} + A1\left(mean_j - x_{i,j}^{t}\right) \times rand(0,1) + A2\left(p_{k,j} - x_{i,j}^{t}\right) \times rand(-1,1), \quad (37)$$

$$A1 = a1 \times exp\left(-\frac{pFit_i}{sumFit + \varepsilon} \times N\right), \quad (38)$$

$$A2 = a2 \times exp\left\{\left(\frac{pFit_i - pFit_k}{|pFit_k - pFit_i| + \varepsilon}\right)\frac{N \times pFit_k}{sumFit + \varepsilon}\right\}, \quad (39)$$

where, positive constants $a1$ and $a2$ are within range [0,2]. $mean_j$ is the average position of $j^{th}$ bird's swarm and $k(k \neq i)$ represents a random nonnegative integer $(k \in \{1, 2, \ldots, N\})$. The *sumFit* is best fitness values sum of birds swarm and $pFit_i$ is $i^{th}$ bird best fitness value. The smallest positive constant $\varepsilon$ is used for avoiding zero division error.

Individual birds travel towards the swarm's center because of indirect and direct effects. The swarm average fitness value is measured in the form of indirect effect and induced by environments. The direct effect is made by specific interference and A2 is used to simulate it. If $k^{th}$ bird $(k \neq i)$ best fitness value is better as compared to $i^{th}$ bird best fitness value, in that case $A2 > a2$. It indicates the $k^{th}$ bird may

suffer a smaller interference as compared to $i^{th}$ bird. Therefore, $k^{th}$ bird would quickly move towards the swarm center as compared to $i^{th}$ bird. However, there are some random movements of birds towards the center of the swarm. In the case of minimizing optimization problems, the bird's smallest fitness value is considered a better fitness value.

### C. FLIGHT BEHAVIOUR

The birds in a swarm have flight behaviour due to foraging behaviour or any other reason. During the flight behaviour the birds in the swarm can be often switched again into two types of birds; 1) producer birds and scrounger birds on the basis of their food reserves (Rule4). The producer behaviours and scrounger behaviour can be written as, respectively [56]:

$$x_{i,j}^{t+1} = x_{i,j}^{t} + randn(0,1) \times x_{i,j}^{t}, \quad (40)$$

$$x_{i,j}^{t+1} = x_{i,j}^{t} + \left(x_{k,j}^{t} - x_{i,j}^{t}\right) \times FL \times rand(0,1), \quad (41)$$

where, $k(k \neq i)$, represents a nonnegative integer ($k \in \{1, 2, \ldots, N\}$). FL is the following coefficient for hunting food – bird's scrounger behaviour (Rule 5). The term $randn(0, 1)$ is random number normal distribution.

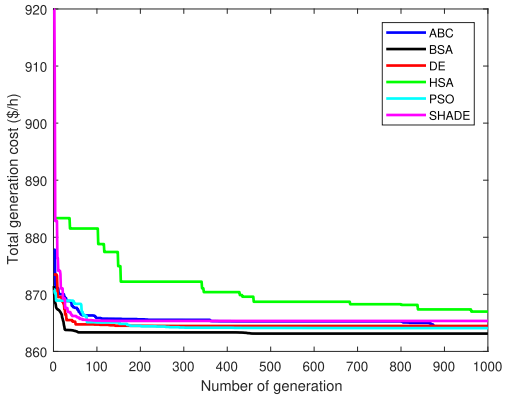


(a) Case 1

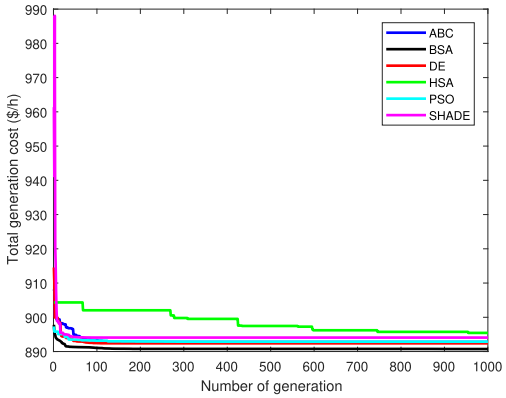


(b) Case 2

**FIGURE 8.** Optimal power generation cost convergence.

## V. SIMULATION RESULTS AND CASE STUDIES

The simulation-based optimization results of the BSA are measured and a comparison is made with other algorithms including harmony search algorithm (HSA), DE, SHADE, PSO, and ABC. For a fair comparison, we used the same number of iterations and parameter settings in BSA approach and other algorithms. For experimental purposes, generator buses voltage magnitude lower and upper limits have been kept [0.95, 1.1] p.u. based on 100 MVA. The voltage magnitudes boundary limits of load or PQ buses have been kept [0.95 1.05]p.u.. The modified IEEE-30 bus test system has 435.0 MW power generation capacity has been utilized for performance evaluation and its further detailed is available in Table 9.

We have implemented the proposed method and other algorithms in MATLAB R2017a and used the MATPOWER6.0

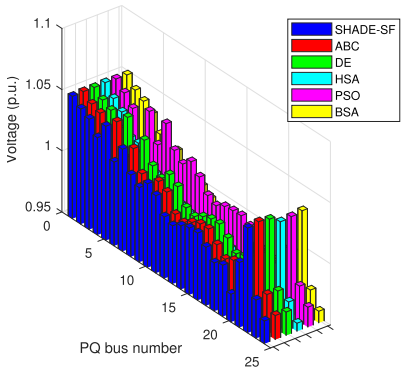


(a) Case 1

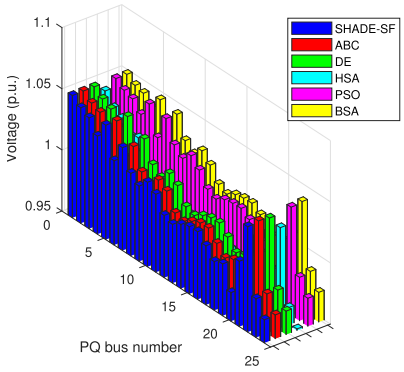


(b) Case 2

**FIGURE 9.** Load or PQ buses voltage magnitude profiles.

**TABLE 9.** The modified IEEE-30 bus test system.

| Variables/Items | Quantity | Details |
|---|---|---|
| Buses | 30 | [64] |
| Branches | 41 | [64] |
| TG ($TG_1, TG_2$) | 2 | Thermal energy sources connected at bus 1 (swing) and 2 |
| Windfarms ($WF_5$, $WF_{11}$) | 2 | Wind energy sources connected at 5 and 11 buses |
| Solar PV units ($SPV_8, SPV_{13}$) | 2 | Solar energy sources connected at 8 and 13 buses |
| Control variables | 11 | Active (real) power of generator buses: $TG_2$, $WF_5, WF_{11}, SPV_8$, and $SPV_{13}$; all generator buses voltage magnitudes |
| Load buses | 24 | In range [0.95 - 1.05] p.u. voltage magnitude based on 100 MVA |

**TABLE 10. Simulation results for electricity generation cost case studies.**

| | | Case study 1 | | | | | | Case study 2 | | | | | |
|---|---|---|---|---|---|---|---|---|---|---|---|---|---|
| Control variables | Range | BSA | SHADE | ABC | DE | HSA | PSO | BSA | SHADE | ABC | DE | HSA | PSO |
| $P_{TG_2}$ (MW) | [20 80] | 37.4850 | 32.3504 | 36.2577 | 33.4091 | 31.8203 | 33.8896 | 36.7974 | 38.4690 | 34.9433 | 37.6030 | 39.9461 | 34.9554 |
| $P_{ws_5}$ (MW) | [0 75] | 42.9392 | 46.1542 | 43.9108 | 46.5344 | 49.8325 | 46.6260 | 48.9397 | 49.1541 | 47.1549 | 48.4909 | 46.4054 | 47.1115 |
| $P_{ws_{11}}$ (MW) | [0 60] | 39.0016 | 38.4922 | 34.5213 | 38.9261 | 34.7548 | 39.1029 | 38.8681 | 40.8279 | 39.3773 | 40.4304 | 38.7578 | 39.3768 |
| $P_{pvs_8}$ (MW) | [0 35] | 26.6732 | 29.1947 | 25.0737 | 25.2941 | 27.4310 | 29.0365 | 28.1425 | 27.2167 | 29.0401 | 28.1857 | 30.9372 | 29.0401 |
| $P_{pvs_{13}}$ (MW) | [0 50] | 36.6868 | 36.9460 | 43.1818 | 38.7837 | 38.8529 | 34.0625 | 39.4787 | 36.8108 | 42.4733 | 37.6525 | 36.1698 | 42.5311 |
| $V_1$ (p.u.) | [0.95 1.1] | 1.1000 | 1.0720 | 1.1000 | 1.1000 | 1.0741 | 1.1000 | 1.1000 | 1.0723 | 1.1000 | 1.1000 | 1.0921 | 1.1000 |
| $V_2$ (p.u.) | [0.95 1.1] | 1.0895 | 1.0571 | 1.0895 | 1.0893 | 1.0155 | 1.0894 | 1.0897 | 0.9500 | 1.0901 | 1.0901 | 0.9947 | 1.0902 |
| $V_5$ (p.u.) | [0.95 1.1] | 1.1000 | 1.0335 | 1.0681 | 1.0685 | 1.0292 | 1.1000 | 1.1000 | 1.0374 | 1.0698 | 1.0699 | 1.0971 | 1.1000 |
| $V_8$ (p.u.) | [0.95 1.1] | 1.0816 | 1.0420 | 1.1000 | 1.0975 | 1.0338 | 1.1000 | 1.0898 | 1.1000 | 1.1000 | 1.1000 | 1.0609 | 1.1000 |
| $V_{11}$ (p.u.) | [0.95 1.1] | 1.0983 | 1.0979 | 1.1000 | 1.1000 | 1.0856 | 1.1000 | 1.0946 | 1.1000 | 1.1000 | 1.1000 | 1.0827 | 1.1000 |
| $V_{13}$ (p.u.) | [0.95 1.1] | 1.0914 | 1.0563 | 1.1000 | 1.0980 | 1.0612 | 1.0998 | 1.1000 | 1.0665 | 1.0995 | 1.0974 | 1.0833 | 1.1000 |
| State variables and parameters | | | | | | | | | | | | | |
| $P_{TG_1}$ (MW) | [50 140] | 134.9079 | 134.9079 | 134.9193 | 134.9079 | 135.6729 | 134.9082 | 124.8093 | 125.1890 | 124.1971 | 125.0028 | 125.5352 | 124.1972 |
| $Q_{TG_1}$ (MVAr) | [-20 150] | -12.4305 | -2.30334 | -12.5176 | -11.9202 | 26.7808 | -13.0004 | -11.1143 | 15.7163 | -11.5389 | -11.3642 | 18.8021 | -12.5837 |
| $Q_{TG_2}$ (MVAr) | [-20 60] | 13.6009 | 13.6284 | 18.8510 | 18.6247 | -20.0000 | 11.0168 | 9.31726 | -20.0000 | 17.3759 | 17.6420 | -20.0000 | 9.9737 |
| $Q_{ws_5}$ (MVAr) | [-30 35] | 35.0000 | 24.0495 | 26.1114 | 25.8388 | 28.3866 | 35.0000 | 35.0000 | 30.8122 | 25.5646 | 25.5455 | 35.0000 | 35.0000 |
| $Q_{ws_{11}}$ (MVAr) | [-25 30] | 18.6602 | 30.0000 | 18.8341 | 19.1880 | 27.3735 | 18.2780 | 16.4646 | 30.0000 | 18.7001 | 18.9821 | 18.4660 | 18.0063 |
| $Q_{pvs_8}$ (MVAr) | [-15 40] | 40.0000 | 35.5230 | 40.0000 | 40.0000 | 34.2617 | 40.0000 | 40.0000 | 40.0000 | 40.0000 | 40.0000 | 40.0000 | 40.0000 |
| $Q_{pvs_{13}}$ (MVAr) | [-20 25] | 20.5446 | 18.2397 | 23.8205 | 23.1885 | 22.8111 | 23.2497 | 23.4645 | 21.9678 | 23.2277 | 22.6629 | 23.5992 | 22.8062 |
| $P_G$ (MW) | | 317.6938 | 318.0454 | 317.8646 | 317.8553 | 318.3644 | 317.6257 | 317.0358 | 317.6674 | 317.1860 | 317.3652 | 317.7514 | 317.2121 |
| $P_D$ (MW) | | 311.63 | 311.63 | 311.63 | 311.63 | 311.63 | 311.63 | 311.63 | 311.63 | 311.63 | 311.63 | 311.63 | 311.63 |
| $P_{loss}$ (MW) | | 6.0638 | 6.4154 | 6.2346 | 6.2253 | 6.7344 | 5.9957 | 5.4058 | 5.8053 | 6.0374 | 5.5560 | 5.7352 | 6.1214 |
| Voltage deviation (p.u.) | | 1.0241 | 0.4696 | 1.0524 | 1.0444 | 0.4493 | 1.1017 | 1.0853 | 0.5044 | 1.0787 | 1.0624 | 0.7096 | 1.1208 |
| Emission (ton/h) | | 1.7080 | 1.7088 | 1.7094 | 1.7086 | 1.7941 | 1.7085 | 0.9071 | 0.9284 | 0.8738 | 0.9179 | 0.9483 | 0.8738 |
| Carbon tax ($/h) | | - | - | - | - | - | - | 18.142 | 18.568 | 17.476 | 18.358 | 18.966 | 17.476 |
| Power generation cost ($/h) | | **863.121** | 865.339 | 864.344 | 864.454 | 866.977 | 864.082 | **890.728** | 894.076 | 892.779 | 892.397 | 895.441 | 892.865 |

package for load flow calculation. The execution of simulation-based experiments have been performed on Microsoft Windows 10 64-bits with Intel Core(TM) i7-5500U CPU @2.40 GHz and RAM @8.00 GB. We have conducted two case studies for performance evaluation of the proposed BSA method. Initially, we have solved the OPF problems in a hybrid power system by considering the objective to reduce electricity generation cost. In second case, carbon tax (e.g., emission cost) is included in power generation cost minimization objective function to reduce emissions pollution.

### A. CASE STUDY 1: GENERATION COST MINIMIZATION

The simulation-based experiments have been conducted for performance evaluation of the BSA-based proposed method and other metaheuristic algorithms to solve the OPF problems in a hybrid power system. The OPF problem objective to reduce the electricity output cost is written in Eq. 23, excluding last term (emission cost or carbon tax). In Eq. 23, the first term $\xi_T(P_{TG})$, represents the power output cost related to thermal energy sources. The second term $\sum_{j=1}^{N_{WF}} \xi_{w,j}(P_{w,j})$ is power output cost related to windfarms and the third term $\sum_{k=1}^{N_{PV}} \xi_{pv,k}(P_{pv,k})$ is power output cost of solar PV units.

The electricity generation cost of an individual windfarm is calculated by adding three types of wind related cost such as 1) wind-scheduled power cost, 2) reserve cost, and 3) penalty cost. Wind-scheduled power cost of an individual windfarm follows a direct relationship to wind-scheduled power and a high spinning reserve is required when wind-scheduled power is kept high. In such a case, overall wind power cost increases while at a lower rate penalty cost decreases. The wind speed and wind electricity generation are highly dependent on the value of scale parameter c of Weibull PDF and the lowest wind power cost achieved at an intermediate value. Similarly, the electricity generation cost of an individual solar PV unit is also calculated by adding penalty cost, reserve cost, and solar-scheduled power cost related to solar PV unit. Solar-scheduled power cost related to solar PV units also follows a direct relationship to solar-scheduled power. It is observed that solar power output cost did not monotonically increase with the values of lognormal PDF parameters such as standard deviation $\sigma$ and mean $\mu$ for solar irradiance. Therefore, serious attention is required to choose the suitable value of solar-scheduled power associated with solar PV units. If the mean $\mu$ value is kept low, then it is suggested to choose a smaller value for solar-scheduled power.

**TABLE 11. Case study 1: Trade-off.**

| Algorithm | Generation cost ($/h) | Convergence time (seconds) | No. of generation |
|---|---|---|---|
| ABC | 864.344 | 1062.0764 | 996 |
| BSA | 863.121 | 503.968 | 508 |
| DE | 864.454 | 329.966 | 428 |
| HSA | 866.977 | 25.953 | 1000 |
| PSO | 864.082 | 686.695 | 817 |
| SHADE | 865.339 | 196.241 | 207 |

In Table 10, optimal values of objective function, parameters, control and state variables obtained from BSA, and other evolutionary algorithms are given, where minimum power output cost is represented in **boldface**. A minimum value of power generation cost **863.121** $/h as specified in Table 10 was obtained in BSA approach and it has outperformed as compared to other metaheuristic algorithms. The optimal power generation cost 864.082 $/h, 864.344 $/h, 864.454 $/h,

865.339 $/h, and 866.977 $/h are obtained using PSO, ABC, DE, SHADE, and HSA, respectively. The optimal power generation cost convergence of the proposed method based on BSA and other metaheuristic algorithms are graphically plotted in Figure 8a. All load or PQ buses voltage magnitude profiles obtained during performance evaluation of BSA and other algorithms are plotted in Figure 9a. For case study 1, the trade-off between optimal power generation cost and convergence time of the BSA-based proposed method and other algorithms are presented in Table 11.

### B. CASE STUDY 2: GENERATION PLUS EMISSION COST MINIMIZATION

In case study 2, the minimum electricity generation cost expressed in Eq. 23 including emission cost (e.g., carbon tax) is an objective function for performance evaluation of the BSA-based proposed method. In this study, a carbon tax rate $C_{tax}$ ($20/ton) is imposed on released $NO_x$, $SO_x$, and $CO_x$ from fossil fuel-based energy sources. It is observed that the generation of the clean form of energy from solar and wind have increased and emission $(ton/h)$ pollution decreased in the power system by imposing a carbon tax.

**TABLE 12. Case study 2: Trade-off.**

| Algorithm | Generation cost + carbon tax ($/h) | Convergence time (seconds) | No. of generation |
|---|---|---|---|
| ABC | 892.779 | 482.718 | 457 |
| BSA | 890.728 | 652.807 | 776 |
| DE | 892.397 | 217.160 | 236 |
| HSA | 895.441 | 25.047 | 898 |
| PSO | 892.865 | 375.016 | 412 |
| SHADE | 894.076 | 168.630 | 153 |

For case study 2, optimum values of objective function related parameters, control variables, and state variables have been specified in Table 10 by applying the proposed BSA method and other algorithms. Simulation results indicate that the BSA outperforms and provides minimum power generation cost **890.728** $/h in case study 2 along with satisfying constraints. The optimal power generation cost 892.397 $/h, 892.779 $/h, 892.865 $/h, 894.076 $/h, and 895.441 $/h are obtained from DE, ABC, PSO, SHADE, and HSA, respectively. For case study 2, the convergence of optimal power generation costs using the proposed BSA method and other algorithms is plotted in Figure 8b. All load or PQ buses voltage magnitude profiles are plotted in Figure 9b. The trade-off between optimal power generation cost and convergence time of proposed method and other algorithms is represented in Table 12. The simulation-based experiment results indicate that power generation from RESs increased when the carbon tax $(ton/h)$ was imposed on carbon emission from fossil fuel-based energy sources.

## VI. CONCLUSION

We have proposed a new bio-inspired bird swarm algorithm for finding optimal solutions to the OPF problems in the traditional thermal, wind, and solar energy sources-based hybrid power system, in this study. In which, we have incorporated utility load demand uncertainty and stochastic nature power generation from RESs. The power generation cost for thermal energy sources is measured using a valve-point loading effects quadratic fuel curve. The Gaussian PDF, Lognormal PDF, and Weibull PDF have been used for modeling uncertainty of utility load demand, stochastic solar irradiance, and wind speed, respectively. The simulation-based optimization results have shown the superiority of the BSA to solve the OPF problems by satisfying all constraints and minimum power generation cost 863.121 $/h is achieved in case study 1. It has been observed from optimization results that the generation of the clean form of energy from RESs has increased and emission pollution has decreased in the hybrid power system by imposing a carbon tax. In case study 2, the proposed BSA approach has also outperformed and minimum electricity cost 890.728 $/h is achieved as compared to other algorithms. The comparative evaluation and simulation-based optimization results confirmed the superiority of BSA approach over other metaheuristic algorithms. The optimization performance of BSA in terms of accuracy, stability, and efficiency have made it attractive for application to real-time optimization problems. The simulation results have encouraged for further study. In future, the application of proposed BSA approach can be extended in a large-scale traditional thermal energy sources-based power system to solve the other optimization problems such as unit commitment, chance-constrained OPF, Transient stability constrained OPF.

## REFERENCES

[1] S. Rahim, N. Javaid, R. D. Khan, N. Nawaz, and M. Iqbal, "A convex optimization based decentralized real-time energy management model with the optimal integration of microgrid in smart grid," *J. Cleaner Prod.*, vol. 236, Nov. 2019, Art. no. 117688.
[2] H. Xiao and M. Cao, "Balancing the demand and supply of a power grid system via reliability modeling and maintenance optimization," *Energy*, vol. 210, Nov. 2020, Art. no. 118470.
[3] L. Gan, P. Jiang, B. Lev, and X. Zhou, "Balancing of supply and demand of renewable energy power system: A review and bibliometric analysis," *Sustain. Futures*, vol. 2, Mar. 2020, Art. no. 100013.
[4] I. Colak, S. Sagiroglu, G. Fulli, M. Yesilbudak, and C.-F. Covrig, "A survey on the critical issues in smart grid technologies," *Renew. Sustain. Energy Rev.*, vol. 54, pp. 396–405, Feb. 2016.
[5] A. F. Attia, R. A. El Sehiemy, and H. M. Hasanien, "Optimal power flow solution in power systems using a novel sine-cosine algorithm," *Int. J. Electr. Power Energy Syst.*, vol. 99, pp. 331–343, Jun. 2018.
[6] A. E. Chaib, H. R. E. H. Bouchekara, R. Mehasni, and M. A. Abido, "Optimal power flow with emission and non-smooth cost functions using backtracking search optimization algorithm," *Int. J. Elect. Power Energy Syst.*, vol. 81, pp. 64–77, Oct. 2016.
[7] S. Frank and S. Rebennack, "An introduction to optimal power flow: Theory, formulation, and examples," *IIE Trans.*, vol. 48, no. 12, pp. 1172–1197, Aug. 2016.
[8] P. P. Biswas, P. N. Suganthan, and G. A. J. Amaratunga, "Optimal power flow solutions incorporating stochastic wind and solar power," *Energy Convers. Manage.*, vol. 148, pp. 1194–1207, Sep. 2017.
[9] S. S. Reddy, "Multi-objective optimal power flow for a thermal-wind-solar power system," *J. Green Eng.*, vol. 7, no. 4, pp. 451–476, Apr. 2018.
[10] K. Zehar and S. Sayah, "Optimal power flow with environmental constraint using a fast successive linear programming algorithm: Application to the Algerian power system," *Energy Convers. Manage.*, vol. 49, no. 11, pp. 3362–3366, Nov. 2008.
[11] P. Fortenbacher and T. Demiray, "Linear/quadratic programming-based optimal power flow using linear power flow and absolute loss approximations," *Int. J. Electr. Power Energy Syst.*, vol. 107, pp. 680–689, May 2019.

[12] S. Mhanna and P. Mancarella, "An exact sequential linear programming algorithm for the optimal power flow problem," *IEEE Trans. Power Syst.*, early access, Jul. 14, 2021, doi: 10.1109/TPWRS.2021.3097066.

[13] H. Ambriz-Perez, E. Acha, and C. R. Fuerte-Esquivel, "Advanced SVC models for Newton-Raphson load flow and Newton optimal power flow studies," *IEEE Trans. Power Syst.*, vol. 15, no. 1, pp. 129–136, Feb. 2000.

[14] B. Liu, J. Li, H. Ma, and Y. Liu, "Generalized benders decomposition based dynamic optimal power flow considering discrete and continuous decision variables," *IEEE Access*, vol. 8, pp. 194260–194268, 2020.

[15] R. S. Salgado and E. L. Rangel, "Optimal power flow solutions through multi-objective programming," *Energy*, vol. 42, no. 1, pp. 35–45, Jun. 2012.

[16] V. Vasylius, A. Jonaitis, S. Gudžius, and V. Kopustinskas, "Multi-period optimal power flow for identification of critical elements in a country scale high voltage power grid," *Rel. Eng. Syst. Saf.*, vol. 216, Dec. 2021, Art. no. 107959.

[17] S. Tu, A. Wachter, and E. Wei, "A two-stage decomposition approach for AC optimal power flow," *IEEE Trans. Power Syst.*, vol. 36, no. 1, pp. 303–312, Jan. 2021.

[18] M. Pourakbari-Kasmaei, M. Lehtonen, M. Fotuhi-Firuzabad, M. Marzband, and J. R. S. Mantovani, "Optimal power flow problem considering multiple-fuel options and disjoint operating zones: A solver-friendly MINLP model," *Int. J. Electr. Power Energy Syst.*, vol. 113, pp. 45–55, Dec. 2019.

[19] F. Capitanescu and L. Wehenkel, "Experiments with the interior-point method for solving large scale optimal power flow problems," *Electr. Power Syst. Res.*, vol. 95, pp. 276–283, Feb. 2013.

[20] H. Wei, H. Sasaki, J. Kubokawa, and R. Yokoyama, "An interior point nonlinear programming for optimal power flow problems with a novel data structure," *IEEE Trans. Power Syst.*, vol. 13, no. 3, pp. 870–877, Aug. 1998.

[21] E. P. de Carvalho, A. dos Santos, and T. F. Ma, "Reduced gradient method combined with augmented Lagrangian and barrier for the optimal power flow problem," *Appl. Math. Comput.*, vol. 200, no. 2, pp. 529–536, Jul. 2008.

[22] X. Yuan, B. Zhang, P. Wang, J. Liang, Y. Yuan, Y. Huang, and X. Lei, "Multi-objective optimal power flow based on improved strength Pareto evolutionary algorithm," *Energy*, vol. 122, pp. 70–82, Mar. 2017.

[23] N. Daryani, M. T. Hagh, and S. Teimourzadeh, "Adaptive group search optimization algorithm for multi-objective optimal power flow problem," *Appl. Soft Comput.*, vol. 38, pp. 1012–1024, Jan. 2016.

[24] K. Abaci and V. Yamacli, "Differential search algorithm for solving multi-objective optimal power flow problem," *Int. J. Electr. Power Energy Syst.*, vol. 79, pp. 1–10, Jul. 2016.

[25] H. R. E. H. Bouchekara, A. E. Chaib, M. A. Abido, and R. A. El-Sehiemy, "Optimal power flow using an improved colliding bodies optimization algorithm," *Appl. Soft Comput.*, vol. 42, pp. 119–131, May 2016.

[26] A.-A. A. Mohamed, Y. S. Mohamed, A. A. M. El-Gaafary, and A. M. Hemeida, "Optimal power flow using moth swarm algorithm," *Electr. Power Syst. Res.*, vol. 142, pp. 190–206, Jan. 2017.

[27] H. Pulluri, R. Naresh, and V. Sharma, "Application of stud krill herd algorithm for solution of optimal power flow problems," *Int. Trans. Electr. Energy Syst.*, vol. 27, no. 6, p. e2316, Jun. 2017.

[28] H. Pulluri, R. Naresh, and V. Sharma, "A solution network based on stud krill herd algorithm for optimal power flow problems," *Soft Comput.*, vol. 22, no. 1, pp. 159–176, Jan. 2018.

[29] P. P. Biswas, P. N. Suganthan, R. Mallipeddi, and G. A. J. Amaratunga, "Optimal power flow solutions using differential evolution algorithm integrated with effective constraint handling techniques," *Eng. Appl. Artif. Intell.*, vol. 68, pp. 81–100, Feb. 2018.

[30] A. Gacem and D. Benattous, "Hybrid genetic algorithm and particle swarm for optimal power flow with non-smooth fuel cost functions," *Int. J. Syst. Assurance Eng. Manage.*, vol. 8, no. S1, pp. 146–153, Jan. 2017.

[31] H. R. E. H. Bouchekara, A. E. Chaib, and M. A. Abido, "Optimal power flow using GA with a new multi-parent crossover considering: Prohibited zones, valve-point effect, multi-fuels and emission," *Electr. Eng.*, vol. 100, no. 1, pp. 151–165, Mar. 2018.

[32] T. T. Nguyen, "A high performance social spider optimization algorithm for optimal power flow solution with single objective optimization," *Energy*, vol. 171, pp. 218–240, Mar. 2019.

[33] M. A. Taher, S. Kamel, F. Jurado, and M. Ebeed, "Modified grasshopper optimization framework for optimal power flow solution," *Elect. Eng.*, vol. 101, no. 1, pp. 121–148, Apr. 2019.

[34] M. A. Taher, S. Kamel, F. Jurado, and M. Ebeed, "An improved moth-flame optimization algorithm for solving optimal power flow problem," *Int. Trans. Elect. Energy Syst.*, vol. 29, no. 3, p. e2743, Mar. 2019.

[35] P. P. Biswas, P. N. Suganthan, R. Mallipeddi, and G. A. J. Amaratunga, "Multi-objective optimal power flow solutions using a constraint handling technique of evolutionary algorithms," *Soft Comput.*, vol. 24, no. 4, pp. 2999–3023, Feb. 2020.

[36] G. Chen, J. Qian, Z. Zhang, and S. Li, "Application of modified pigeon-inspired optimization algorithm and constraint-objective sorting rule on multi-objective optimal power flow problem," *Appl. Soft Comput.*, vol. 92, Jul. 2020, Art. no. 106321.

[37] H. Buch and I. N. Trivedi, "An efficient adaptive moth flame optimization algorithm for solving large-scale optimal power flow problem with POZ, multifuel and valve-point loading effect," *Iranian J. Sci. Technol., Trans. Electr. Eng.*, vol. 43, no. 4, pp. 1031–1051, Dec. 2019.

[38] R. Roy and H. T. Jadhov, "Optimal power flow solution of power system incorporating stochastic wind power using Gbest guided artificial bee colony algorithm," *Int. J. Elect. Power Energy Syst.*, vol. 64, pp. 562–578, Jan. 2015.

[39] A. Panda and M. Tripathy, "Optimal power flow solution of wind integrated power system using modified bacteria foraging algorithm," *Int. J. Elect. Power Energy Syst.*, vol. 54, pp. 306–314, Jan. 2014.

[40] A. Panda and M. Tripathy, "Security constrained optimal power flow solution of wind-thermal generation system using modified bacteria foraging algorithm," *Energy*, vol. 93, pp. 816–827, Dec. 2015.

[41] S. R. Salkuti, "Optimal power flow using multi-objective glowworm swarm optimization algorithm in a wind energy integrated power system," *Int. J. Green Energy*, vol. 16, no. 15, pp. 1547–1561, Dec. 2019.

[42] L. Shi, C. Wang, L. Yao, Y. Ni, and M. Bazargan, "Optimal power flow solution incorporating wind power," *IEEE Syst. J.*, vol. 6, no. 2, pp. 233–241, Jun. 2012.

[43] I. U. Khan, N. Javaid, K. A. A. Gamage, C. J. Taylor, S. Baig, and X. Ma, "Heuristic algorithm based optimal power flow model incorporating stochastic renewable energy sources," *IEEE Access*, vol. 8, pp. 148622–148643, 2020.

[44] M. A. Ilyas, G. Abbas, T. Alquthami, M. Awais, and M. B. Rasheed, "Multi-objective optimal power flow with integration of renewable energy sources using fuzzy membership function," *IEEE Access*, vol. 8, pp. 143185–143200, 2020.

[45] S. Li, W. Gong, L. Wang, X. Yan, and C. Hu, "Optimal power flow by means of improved adaptive differential evolution," *Energy*, vol. 198, May 2020, Art. no. 117314.

[46] J. Ben Hmida, T. Chambers, and J. Lee, "Solving constrained optimal power flow with renewables using hybrid modified imperialist competitive algorithm and sequential quadratic programming," *Electr. Power Syst. Res.*, vol. 177, Dec. 2019, Art. no. 105989.

[47] E. E. Elattar and S. ElSayed, "Modified JAYA algorithm for optimal power flow incorporating renewable energy sources considering the cost, emission, power loss and voltage profile improvement," *Energy*, vol. 178, pp. 598–609, Jul. 2019.

[48] Z. Ullah, S. Wang, J. Radosavljević, and J. Lai, "A solution to the optimal power flow problem considering WT and PV generation," *IEEE Access*, vol. 7, pp. 46763–46772, 2019.

[49] M. H. Sulaiman and Z. Mustaffa, "Optimal power flow incorporating stochastic wind and solar generation by metaheuristic optimizers," *Microsyst. Technol.*, vol. 27, pp. 3263–3277, Oct. 2020.

[50] T. Samakpong, W. Ongsakul, and N. Madhu Manjiparambil, "Optimal power flow incorporating renewable uncertainty related opportunity costs," *Comput. Intell.*, to be published.

[51] S. Duman, S. Rivera, J. Li, and L. Wu, "Optimal power flow of power systems with controllable wind-photovoltaic energy systems via differential evolutionary particle swarm optimization," *Int. Trans. Elect. Energy Syst.*, vol. 30, no. 4, Apr. 2020, Art. no. e12270.

[52] A. Panda, U. Mishra, M.-L. Tseng, and M. H. Ali, "Hybrid power systems with emission minimization: Multi-objective optimal operation," *J. Cleaner Prod.*, vol. 268, Sep. 2020, Art. no. 121418.

[53] M. A. M. Shaheen, H. M. Hasanien, S. F. Mekhamer, and H. E. A. Talaat, "Optimal power flow of power systems including distributed generation units using sunflower optimization algorithm," *IEEE Access*, vol. 7, pp. 109289–109300, 2019.

[54] A. M. Shaheen, R. A. El-Sehiemy, and S. M. Farrag, "Solving multi-objective optimal power flow problem via forced initialised differential evolution algorithm," *IET Gener., Transmiss. Distrib.*, vol. 10, no. 7, pp. 1634–1647, May 2016.

[55] A. R. Bhowmik and A. K. Chakraborty, "Solution of optimal power flow using non dominated sorting multi objective opposition based gravitational search algorithm," *Int. J. Elect. Power Energy Syst.*, vol. 64, pp. 1237–1250, Jan. 2015.
[56] X.-B. Meng, X. Z. Gao, L. Lu, Y. Liu, and H. Zhang, "A new bio-inspired optimisation algorithm: Bird swarm algorithm," *J. Exp. Theor. Artif. Intell.*, vol. 28, pp. 673–687, Jun. 2015.
[57] M. Ahmad, N. Javaid, I. A. Niaz, S. Shafiq, O. U. Rehman, and H. M. Hussain, "Application of bird swarm algorithm for solution of optimal power flow problems," in *Proc. Conf. Complex, Intell., Softw. Intensive Syst.*, Matsue, Japan, Jul. 2018, pp. 280–291.
[58] T. P. Chang, "Investigation on frequency distribution of global radiation using different probability density functions," *Int. J. Appl. Sci. Eng.*, vol. 8, no. 2, pp. 99–107, Sep. 2010.
[59] F. Yao, Z. Y. Dong, K. Meng, Z. Xu, H. H.-C. Iu, and K. P. Wong, "Quantum-inspired particle swarm optimization for power system operations considering wind power uncertainty and carbon tax in Australia," *IEEE Trans. Ind. Informat.*, vol. 8, no. 4, pp. 880–888, Nov. 2012.
[60] M. Ebeed and S. H. Aleem, "Overview of uncertainties in modern power systems: Uncertainty models and methods," *Uncertainties in Modern Power Systems*. New York, NY, USA: Academic, 2021, pp. 1–34. Accessed: Oct. 28, 2021. [Online]. Available: https://www.sciencedirect.com/book/9780128204917/
[61] H. P. Hong, "An efficient point estimate method for probabilistic analysis," *Rel. Eng. Syst. Saf.*, vol. 59, no. 3, pp. 261–267, 1998.
[62] M. Aien, A. Hajebrahimi, and M. Fotuhi-Firuzabad, "A comprehensive review on uncertainty modeling techniques in power system studies," *Renew. Sustain. Energy Rev.*, vol. 57, pp. 1077–1089, May 2016.
[63] X. Li, J. Cao, and D. Du, "Probabilistic optimal power flow for power systems considering wind uncertainty and load correlation," *Neurocomputing*, vol. 148, pp. 240–247, Jan. 2015.
[64] S. Shargh, B. K. Ghazani, B. Mohammadi-Ivatloo, H. Seyedi, and M. Abapour, "Probabilistic multi-objective optimal power flow considering correlated wind power and load uncertainties," *Renew. Energy*, vol. 94, pp. 10–21, Aug. 2016.

**MANZOOR AHMAD** received the master's degree in computer science from Quaid-i-Azam University, Islamabad, Pakistan, in 2002, and the master's degree in computer science from Mälardalens högskola Eskilstuna Västerås, Sweden, in 2010. He is currently pursuing the Ph.D. degree in computer science with COMSATS University Islamabad, Islamabad, under supervision of Dr. Iftikhar Azim Niaz and co-supervision of Dr. Nadeem Javaid. Since 2003, he has been associated with COMSATS University Islamabad. He has three research publications in well reputed international conferences. His research interests include artificial intelligence and optimal power flow.

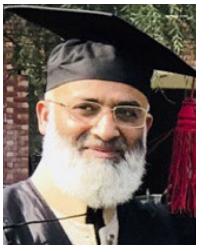

**NADEEM JAVAID** (Senior Member, IEEE) received the bachelor's degree in computer science from Gomal University, Dera Ismail Khan, Pakistan, in 1995, the master's degree in electronics from Quaid-i-Azam University, Islamabad, Pakistan, in 1999, and the Ph.D. degree from the University of Paris-Est, France, in 2010. He is currently an Associate Professor and the Founding Director of the Communications Over Sensors (ComSens) Research Laboratory, Department of Computer Science, COMSATS University Islamabad, Islamabad. He is also working as a Visiting Professor with the School of Computer Science, University of Technology Sydney, Sydney, Australia. He has supervised 137 master and 24 Ph.D. theses. He has authored over 900 articles in technical journals and international conferences. His research interests include energy optimization in smart grids and in wireless sensor networks using data analytics and blockchain. He was a recipient of the Best University Teacher Award from the Higher Education Commission of Pakistan, in 2016, and the Research Productivity Award from the Pakistan Council for Science and Technology, in 2017. He is also an Associate Editor of IEEE Access and an Editor of *Sustainable Cities and Society* journals.

**IFTIKHAR AZIM NIAZ** (Senior Member, IEEE) is currently a Professional Engineer and an Assistant Professor, and the Ph.D. Coordinator with the Department of Computer Science. He has been coordinating with different government and private sectors and organizations, improving the academic standard of students. He has been the Ph.D. Supervisor of the HEC, since 2007. Because of his professional experience, expertise, social and communication skills, he has been on the expert panel of the PEC Accreditation Team, since 2009. He is also a member of various national and international professional bodies and clubs that is one of the necessary conditions for managing projects. His research interests include wireless sensor networks, energy optimization in smart grids, and software engineering.

**AHMAD ALMOGREN** (Senior Member, IEEE) received the Ph.D. degree in computer science from Southern Methodist University, Dallas, TX, USA, in 2002. He is currently a Professor with the Computer Science Department, College of Computer and Information Sciences (CCIS), King Saud University (KSU), Riyadh, Saudi Arabia, where he is also the Director of the Cyber Security Chair, CCIS. Previously, he worked as the Vice Dean of the Development and Quality at CCIS. He also worked as the Dean of the College of Computer and Information Sciences and the Head of the Academic Accreditation Council, Al Yamamah University. His research interests include mobile-pervasive computing and cyber security. He served as the General Chair for the IEEE Smart World Symposium and a Technical Program Committee Member of numerous international conferences/workshops, such as IEEE CCNC, ACM BodyNets, and IEEE HPCC.

**AYMAN RADWAN** (Senior Member, IEEE) received the Ph.D. degree from Queen's University, Kingston, ON, Canada, in 2009. He is currently a Senior Research Engineer (Investigador Auxiliar) with the Instituto de Telecomunicações, University of Aveiro, Aveiro, Portugal. He is mainly specialized in coordination and management of EU funded projects. He participated in the coordination of multiple EU projects. He is also the Project Coordinator of the CELTIC+ Project "MUSCLES," and participating in the coordination of ITN-SECRET. He has also been the Technical Manager of the FP7-C2POWER Project and the Coordinator of the CELTIC+ "Green-T" Project. His current research interests include the Internet of Things, 5G, and green communications.